Approved for public release; distribution is unlimited.

Trailing Vortex Free-Surface Interaction

by

Donald E. Neubert, Jr.
Lieutenant, United States Navy
B.C.E., Villanova University, 1985

Submitted in partial fulfillment of the
requirements for the degree of

MASTER OF SCIENCE IN MECHANICAL ENGINEERING

from the

NAVAL POSTGRADUATE SCHOOL

December 1992

Unclassified
Security Classification of this page

REPORT DOCUMENTATION PAGE

1a Report Security Classification: Unclassified		1b Restrictive Markings	
2a Security Classification Authority		3 Distribution Availability of Report: Approved for public release; distribution unlimited.	
2b Declassification/Downgrading Schedule			
4 Performing Organization Report Number(s)		5 Monitoring Organization Report Number(s)	
6a Name of Performing Organization: Naval Postgraduate School	6b Office Symbol (*If Applicable*): ME	7a Name of Monitoring Organization: Naval Postgraduate School	
6c Address (*city, state, and ZIP code*): Monterey, CA 93943-5000		7b Address (*city, state, and ZIP code*): Monterey, CA 93943-5000	
8a Name of Funding/Sponsoring Organization	8b Office Symbol (*If Applicable*)	9 Procurement Instrument Identification Number	
8c Address (*city, state, and ZIP code*)		10 Source of Funding Numbers	
		Program Element Number	Project No / Task No / Work Unit Accession No

11 Title (*Include Security Classification*)
TRAILING VORTEX / FREE-SURFACE INTERACTION

12 Personal Author(s): DONALD E. NEUBERT, Jr.

13a Type of Report	13b Time Covered	14 Date of Report (*year, month, day*)	15 Page Count
Master of Science Thesis	From: To:	December 1992	81

16 Supplementary Notation: The views expressed in this thesis are those of the author and do not reflect the official policy or position of t Department of Defense or the U. S. Government.

17 Cosati Codes			18 Subject Terms (*continue on reverse if necessary and identify by block number*)
Field	Group	Subgroup	Trailing Vortices, Surface Disturbances, Scars, Striations, Vortex Dynamics, Velocity and Turbulence Measurements

19 Abstract (*continue on reverse if necessary and identify by block number*

An investigation of the interaction of a trailing vortex with a free surface has been undertaken for the purpose of understanding the origin of scars and striations. Velocity and turbulence measurements have been carried out through the use of a Laser-Doppler-Velocimeter (LDV) for various positions of the vortex relative to the free surface. The results have shown that the vortex motion affects the free surface and is affected by it. This mutual interaction leads to the development of surface scars comprised primarily of heterostrophic vortices normal to the free surface. Furthermore, the velocity and turbulence characteristics are affected such that the vertical components of turbulence decay rapidly and the horizontal components stretch in the horizontal plane. The experiments have provided sufficient understanding of the physics of the phenomenon for the subsequent undertaking of the development of a predictive numerical model.

20 Distribution/Availability of Abstract	21 Abstract Security Classification	
[X] unclassified/unlimited [ ] same as report [ ] DTIC users	Unclassified	
22a Name of Responsible Individual: Professor T. Sarpkaya	22b Telephone (*Include Area code*): (408) 646-3425	22c Office Symbol: ME-SL

DD FORM 1473, 84 MAR — 83 APR edition may be used until exhausted; All other editions are obsolete — security classification of this pag

Unclassifie

ABSTRACT

An investigation of the interaction of a trailing vortex with a free surface has been undertaken for the purpose of understanding the origin of scars and striations. Velocity and turbulence measurements have been carried out through the use of a Laser-Doppler-Velocimeter (LDV) for various positions of the vortex relative to the free surface. The results have shown that the vortex motion affects the free surface and is affected by it. This mutual interaction leads to the development of surface scars comprised primarily of heterostrophic vortices normal to the free surface. Furthermore, the velocity and turbulence characteristics are affected such that the vertical components of turbulence decay rapidly and the horizontal components stretch in the horizontal plane. The experiments have provided sufficient understanding of the physics of the phenomenon for the subsequent undertaking of the development of a predictive numerical model.

TABLE OF CONTENTS

LIST OF FIGURES

LIST OF SYMBOLS

b_0	Initial distance between the two vortices
H	$= h_1/h_0$
h_0	Vertical position of the vortex
h_1	Depth of the horizontal plane
R_0	Core radius of the main vortex
Tu	Turbulence intensity
t	Time
U_0	Velocity of the ambient flow
u	Axial velocity
u', v'	Fluctuating components of velocity
v	Vertical velocity
V_0	Maximum velocity in the vortex
X	$= x/\sigma_0$
x	Lateral coordinate
z	The position of the real vortex
Γ	Circulation of the vortex
κ	Normalized circulation
δ	The cut-off distance
Σ	σ_0/h_0
σ	Core radius
ν	Kinematic viscosity
ω	Vorticity

ACKNOWLEDGMENTS

The author wishes to express his sincere appreciation to Distinguished Professor Sarpkaya for his infinite amount of guidance and time. It has been an honor and privilege to conduct research under the expertise of Professor Sarpkaya. I consider the laboratory studies to be one of my most rewarding lifetime opportunities.

I would like to express a special thanks to Mr. Jack McKay for his invaluable work in setting up the laboratory equipment.

Finally, I wish to thank my wife, Claire, for her wonderful support during my thesis work and for our entire stay at the Naval Postgraduate School.

I. INTRODUCTION

The unsteady flow phenomena resulting from the interaction of wakes and vortices with the environment and, in particular, with the free surface are of far-reaching consequence in naval hydrodynamics. They limit the speed, range, stability, and quiet operation of naval vessels, ordnance, and other underwater objects; the ability to detect or conceal acoustic signals while underway; and diverse ocean engineering operations on and under the sea. Equally important is the understanding of the dynamics of interfacial vorticity, particularly the production and sustenance of free surface turbulence. It is because of these reasons that the wake/free-surface interaction and the mechanisms that affect the direct as well as remote observation of ship wakes have become major research topics in hydrodynamics.

An ascending vortex pair produces a three-dimensional complex signature, comprised of a narrow dark band bordered by two bright lines in synthetic-aperture-radar (SAR) images. A few facts are known about them: Their physics is elusive; they are by no means easily accessible to precise measurement; they are not related, at least directly, to the Kelvin wake; and they do not reflect the incident electro-magnetic waves back to the source (negative spectral perturbation). Various proposals have been advanced to provide a feasible explanation of the dark band: Interaction of the wake of a vortex couple with the free surface; turbulence and surface mean flow resulting from the ship's motion; redistribution of surface impurities by large-scale vortical motions, as in Langmuir (1938) circulations and Reynolds

ridges (see, e.g., Scott, 1982); entrained air in the wake; bubble scavenging of surface and subsurface surfactant materials; and the interaction of Kelvin waves, ambient waves, and momentum wake, just to name a few of the existing proposals. Each model attempts to provide a more feasible explanation of the dark narrow band seen in the SAR images (Sarpkaya & Suthon, 1991).

Turbulent flow near surfaces is not uncommon and there has been intense interest in understanding the behavior of vortices near a wall and the physics of the mechanisms sustaining the turbulent behavior (Harvey & Perry, 1971; Smith et al., 1991; Peace & Riley, 1983). Thus, it is not surprising that there should be turbulent flows at and near deformable surfaces or fluid interfaces, in addition to various types of waves, due to complex ship wakes. What is rather surprising is that the resulting turbulent motion should give rise to coherent structures capable of absorbing the incident electromagnetic waves (negative spectral perturbation) for unexpectedly long times even under real ocean ambient conditions. This leads to two generic questions regarding the behavior of turbulence at the free surface: (1) How are the coherent structures created at the interface and what dynamical processes are responsible for their life cycle? (2) What characteristics of these structures (e. g., scale, shape, motion, mutual interaction) are responsible for the absorption of the incident electromagnetic waves? This report is concerned only with the first question. Both the dynamical behavior, through vortex dynamics, and the etiology of the coherent structures (what physical phenomenon causes them), through measurements, are investigated in as much detail as possible.

II. BACKGROUND

Controlled laboratory experiments on free surface structures were first conducted by Sarpkaya in October, 1983, as a continuation of his work on trailing vortices in homogeneous and density stratified media (Sarpkaya, 1983). These observations and measurements were reported by Sarpkaya and Henderson (1984, 1985) and by Sarpkaya (1985, 1986). They have shown that the striations are essentially three-dimensional free-surface disturbances, normal to the direction of motion of the lifting surface. The scars are small free-surface depressions, comprised of many randomly distributed whirls (normal vorticity connecting with the free surface), and come into existence towards the end of the pure striation phase. When the vortices migrate large distances upward, they undergo various types of instabilities. During their formation process, the tightly spiraled regions of each vortex exhibit velocity jumps between the vortex sheets. They are then liable to helical instabilities, even to Helmholtz-type instability, depending on the initial disturbances, Reynolds number, and the entire shape of the generating body (tip shape, cross section, aspect ratio, etc.). The Helmholtz waves on the vortex sheet quickly degenerate into turbulence which encroaches upon the external potential flow. There is considerable disagreement regarding the asymmetry or the axisymmetry of the resulting trailing vortex (Higuchi, et al., 1987; Stinebring, et al., 1989; Green & Acosta, 1991).

Several theories have been proposed to explain the instabilities associated with the trailing vortices: Crow instability (Crow, 1970), Moore and Saffman instability (Moore & Saffman, 1973), Batchelor's (1964) swirling flow

instability, Singh and Uberoi's (1976) helical mode instability, and the free-stream turbulence proposals of Corsiglia et al. (1973) and Baker et al. (1974). Only the helical instabilities proposed by Singh and Uberoi (1976) and observed by Sarpkaya (1985) appear to provide a satisfactory explanation. As noted recently by Bandyopadhyay et al. (1990), the vortex core is not a benign solid body of rotation. "The exchange of momentum between the outer region and the core is carried out by organized motions." It is this exchange of **momentum that leads to the oscillation of the vortex core and the various velocity components.**

A vortex couple usually undergoes both short–wavelength and long–wavelength sinusoidal instability (Crow, 1970), in addition to those cited above, and often breaks up into isolated inclined rings. The interaction of these rings with the free surface gives rise to crescent-shaped scars with many small vortices and to two or more large whirls. As noted by Sarpkaya and Henderson (1984), these "**correspond to local surface depressions where the legs of the broken vortex ring (resembling the legs of an embryonic horseshoe) touch the free surface and relink with their mirror images.**" This phenomenon has been rediscovered five years later by Kwon (1989) who investigated the interaction of vortex rings with the free surface at inclined incidence for clean surface conditions. He too has found that at high angles of incidence the vortex lines in the ring break and reconnect with the surface during the interaction resulting in the formation of horseshoe-shaped vortical regions with legs attached to the surface.

Sarpkaya and Henderson's (1984) and Sarpkaya's (1985) earliest theoretical model of the scar cross-section created by the trailing vortices was

based on the classical solution of Lamb (1945), assuming the vortices to be two-dimensional and the free surface to be a rigid plane. For small Froude numbers F (= $V_o/\sqrt{gb_o}$, where V_o is the initial mutual induction velocity of the vortex couple, and b_o, their initial separation), the vortices follow the simple path described by Lamb's potential-flow solution, the free surface remains fairly flat, and each scar front approximately coincides with the stagnation point on the Kelvin oval, formed by one of the trailing vortices and its image.

Subsequently, Elnitsky (1987) and Sarpkaya et al. (1988) used a novel counter-rotating plate arrangement to generate vortex pairs to study the normal incidence of a two-dimensional vortex pair with the free surface. However, the two-dimensional vortex pair did not lead to a two-dimensional free-surface deformation and, instead, led to the confirmation of the observations made earlier with the inclined trailing vortices that the vortices (inclined or normal) give rise to three-dimensional structures: **scars and striations** (Sarpkaya & Suthon, 1991a, 1991b). Sarpkaya and Suthon (1991a, 1991b) have shown conclusively that the striations are the manifestation of subsurface vortex instabilities that occur whether or not a free surface is present. Furthermore, it was found that for Froude numbers larger than about 0.15, not only the deformation of the free surface but also the nonlinear interaction between the said deformation and the motion of the vortices become significant. The vortices follow Lamb's solution only during the early stages of their rise. Subsequently, they exhibit paths of varying degrees of complexity, depending on F and the Reynolds number Re = $V_o b_o/\nu$. For example, for F = 0.6 the vortices rise vertically upward and, instead of moving

away from the center, move initially toward the center line as they are drawn up into the domed region created by their rise.

Numerical simulations of the domed region, formed by the rise of a Kelvin oval, attracted considerable attention. Sarpkaya et al. (1988) modeled the vortex pair using two point vortices (with small cores) and line vortices to model the free surface without linearization. Subsequently, Marcus and Berger (1989), Telste (1989), and Ohring and Lugt (1991) used different two-dimensional models to investigate the interaction between a couple of heterostophic line vortices and a free, initially planar, surface. In these calculations, the critical time at which the numerical instability manifests itself does not correspond to the instability of the free surface or to its maximum position. The calculations of Ohring and Lugt are particularly noteworthy since they have presented results on the decay of the primary vortices and their paths, on the generation of surface vorticity and secondary vortices, on the development and final stages of the disturbed free surface, and on the influence of surface tension. They have also shown that, for an intermediate Froude number, the path of the primary vortex center portrays a complete loop (a special rebounding) due to the presence of secondary vortices .

Dommermuth and Yue (1991) solved the linearized Navier-Stokes equations in three dimensions with a free surface to study the interaction of vortex tubes and vortex rings with slip- and no-slip rigid boundaries and a linearized free surface. Subsequently, Dommermuth (1992) carried out numerical simulations of the interaction of laminar vortex tubes with no-slip walls to investigate the formation of U-shaped vortices without the

complications of a free surface. They have concluded that two distinct types of vortices form: cam and snail vortices, as they preferred to call them. Cam vortices are formed as helical vorticity is stripped off of the primary vortex tubes. The helical vortex sheets are generated by the primary vortex tube due to the onset of a U-shaped instability previously identified by Sarpkaya (1985) and by Sarpkaya and Suthon (1991a, 1991b). According to Dommermuth, the rotating rockers of the cam vortices, which are comprised of cross-axis vorticity, cause the unsteady striations in the free surface. As the cam vortices rotate near the free surface, the rotations of the rockers are arrested by the free-surface boundary layer, and this leads to the formation of snail vortices. Snail vortices do not rotate around the primary vortex tubes. Their normal connection with the free surface yields strong whirls.

Evidently, there are a number of additional parameters which might affect the free-surface/vorticity interaction: soluble and insoluble surfactants at the free surface, turbulence, waves, currents, and wind, just to name a few. Hirsa et al. (1991), among others, considered the effect of known surfactants on the flow field during the laminar interaction of a pair of vortices at low Froude and Reynolds numbers. They have concluded that for high Froude numbers the effect of surface contamination might not be as great as it is for vortices with lower Froude numbers. Hirsa et al. (1991) also noted that "in the far wake of ships, which are observed in the SAR images, the turbulence is decaying and the Froude number for the eddies is relatively small and therefore surface contamination plays an important role in the interaction of the eddies with the free surface." Hirsa et al. did not deal with turbulent

vortices. Their Reynolds number was about 12,000 and the Froude number was about 0.2.

The interaction of jet flows with free surfaces has attracted some attention during the past three or four decades (Evans 1955; Ramberg et al. 1989) for the expressed purpose of determining the topology and the dynamics of the turbulent structures resulting from the interaction of a free jet with the free surface. More recently, Madnia and Bernal (1989) and Anthony (1990) carried out extensive LDV measurements with round jets for the purpose of delineating the characteristics of vortical structures interacting with the free surface. The results have confirmed those deduced from previous investigations (Ramberg et al., 1989; Komori et al., 1982) that the RMS velocity fluctuations parallel to the surface are enhanced, while those normal to the surface are diminished, thus rendering turbulence more anisotropic as the free surface is approached. Although very instructive in understanding the conversion of the azimuthal vorticity (vortex rings) into streamwise vorticity, the jet flow is neither as complicated as the ship wake nor representative of the turbulent phenomena that occur in the ocean environment partly because there is no normal vorticity generation in the nominal plane of the free surface.

It is clear from the foregoing that a number of kernel experiments, supported by analysis, is needed to elucidate the basic fluid mechanics of turbulent signatures. It is believed that one of the fundamental flows relevant to the dynamical processes in vorticity/free-surface interaction which can be carefully studied in isolation, without complications and competing influences that normally occur in a fully turbulent ship wake, is

the interaction of a single turbulent vortex (and its image) with the free surface. It is this belief that led to the present investigation.

In the following, first the theoretical models used for the characterization of the vortex, then the description of the experimental equipment and procedures, and then the discussion of results and conclusions are presented. The large number of figures generated in the course of the investigation are presented in Appendix A.

III. THEORETICAL MODELS

A. VORTEX MODELS

Here only a brief description of the most representative velocity distributions and their use in the prediction of the vertical component of the vortical velocity at a given elevation below the free surface are described.

The ideal line vortex (a straight vortex filament of non-zero circulation, vanishing cross-section, and infinite vorticity) gives rise to infinitely large velocities at the vortex center and is not representative of a real vortex, i.e., real vortices are not concentrated singularities of infinite vorticity. The best known among the numerous representations of real vortices are the Rankine and Lamb (Oseen) vortices and their suitable modifications.

The Rankine vortex rotates as a solid body within its core and is characterized by a potential flow outside, i.e., all of the vorticity is confined to the core region $r = \sigma$ (i.e., into the so-called compact support). The tangential velocity distribution for an isolated Rankine vortex of normalized strength κ, $(=\Gamma/2\pi)$, has the form,

$$v = \kappa / r \quad \text{for} \quad r > \sigma \tag{1a}$$

$$v = \kappa r / \sigma^2 \quad \text{for} \quad r < \sigma \tag{1b}$$

with an artificial discontinuity at $r = \sigma$. In terms of complex variables, the velocity at an arbitrary point z_k due to a Rankine vortex at z_j may be written as

$$u_k + iv_k = i\kappa_j \frac{z_k - z_j}{r_{jk}^2} \qquad \text{for } r_{jk} = |z_j - z_k| > \sigma \tag{2}$$

and as

$$u_k + iv_k = \frac{i\kappa_j}{\sigma^2}(z_k - z_j) \qquad \text{for } r_{jk} < \sigma, \tag{3}$$

The Rankine model gives rise to a sharp velocity change at $r = \sigma$, from a linear distribution for $r < \sigma$ to a potential velocity distribution for $r > \sigma$. However useful, such an idealization does not exactly represent the behavior of a turbulent trailing vortex.

The Lamb model involves a Gaussian vorticity distribution and a circumferential velocity given by,

$$\omega(r,t) = (\kappa_0/2\pi\nu t)\exp(-r^2/4\nu t) \tag{4}$$

and

$$v(r,t) = (\kappa_0/r)\,[1 - \exp(-r^2/4\nu t)] \tag{5}$$

in which ω is the vorticity, κ_0 is the circulation, r is the radial distance, ν is the kinematic viscosity, and t is the time. Equation (5) is an exact solution of the Navier-Stokes equations for *a single viscous vortex in an unbounded incompressible domain* and $\sqrt{2\nu t} = \sigma$ is the standard deviation of the vorticity distribution. The radius at which the tangential velocity reaches a maximum is $r_m = 2.24\sqrt{\nu t} = 1.584\,\sigma$. The Lamb model is for a laminar vortex and is not expected to represent a turbulent vortex with sufficient accuracy.

Real vortices neither exhibit velocity jumps as in the case of a Rankine vortex nor have all of their vorticity confined to the core. In fact, the character of a real vortex is determined, to a large extent, by the fraction of

vorticity within the core. It is this realization that led Rosenhead (1930) to propose the following velocity distribution:

$$u - iv = -i\kappa\left[\frac{1}{(z+ih_o)}\frac{(z+ih_o)^2}{\left[(z+ih_o)^2+\delta^2\right]}\right] \tag{6}$$

The introduction of δ to the denominator disingularizes the velocity and allows for the matching of the measured and calculated velocity profiles. Clearly, the purpose of δ is not only the disingularization of the velocity at the origin but also the adjustment of the fraction of the total vorticity assigned to the core.

B. VELOCITY DISTRIBUTIONS

Figure 1 shows an idealized trailing vortex at $z = -ih_o$, its image through a rigid but slip-free boundary at $z = +ih_o$, and an arbitrary plane at $z = -ih_1$. The objective is to calculate the v-component of the velocity induced at $z = -ih_1$ through the use of the vortex models described above.

For two potential or Rankine vortices ($|h_o - h_1| > \sigma$), one has

$$F(z) = -i\kappa Ln(z+ih_o) + i\kappa Ln(z-ih_o) \tag{7}$$

which yields

$$\frac{dF}{dz} = u - iv = -i\kappa\left[\frac{1}{z+ih_o} - \frac{1}{z-ih_o}\right] \tag{8}$$

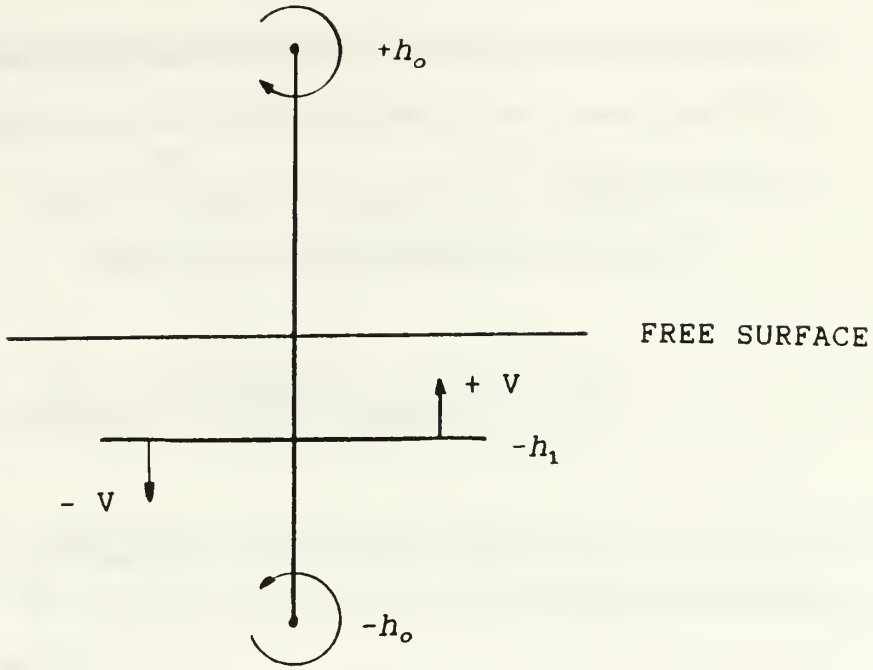

Figure 1. Definition Sketch

Carrying out the indicated calculations, one has

$$v = \frac{4\kappa h_o h_1 x}{\left[x^2 + (h_1 - h_o)^2\right]\left[x^2 + (h_1 + h_o)^2\right]} \tag{9}$$

or in normalized form as,

$$\frac{v}{v_o} = \frac{4HX\Sigma^2}{\left[X^2\Sigma^2 + (H-1)^2\right]\left[X^2\Sigma^2 + (H+1)^2\right]} \tag{10}$$

in which v_o is the measured maximum velocity at the edge of the core of the real vortex, $H = h_1/h_o$, $X = x/\sigma_o$, $\Sigma = \sigma_o/h_o$, and σ_o is the core radius of the real vortex. For $|h_o - h_1| > \sigma$ there is no difference between the velocity fields induced by a potential vortex and a Rankine vortex. The comparisons

between the measured and calculated velocity profiles through the use of Eq. (10) have shown that the Rankine model is not a suitable representation of a turbulent vortex.

The use of two Rosenhead vortices yields,

$$u - iv = -\frac{i\kappa}{(z+ih_o)}\frac{(z+ih_o)^2}{\left[(z+ih_o)^2+\delta^2\right]} + \frac{i\kappa}{(z-ih_o)}\frac{(z-ih_o)^2}{\left[(z-ih_o)^2+\delta^2\right]} \tag{11}$$

in which $\delta = \sigma_o$, the core radius. Extracting the v-component and normalizing, one has

$$\frac{v}{v_o} = \frac{2X\Sigma^2}{\left[X^2\Sigma^2+(1-H)^2+\Sigma^2\right]} - \frac{2X\Sigma^2}{\left[X^2\Sigma^2+(1+H)^2+\Sigma^2\right]} \tag{12}$$

The velocity distribution resulting from this expression matches quite well with that measured through the core of a vortex situated at $h_o = 8.3\sigma_o$ below the free surface, i.e., for a vortex which is sufficiently far from the free surface so as not to be materially affected by the surface disturbances.

However, for a vortex close enough to the free surface (h_o/σ_o less than about 4) where the velocity distribution will be affected by the surface signatures, the use of a Rosenhead type velocity distribution did not prove to be successful. A careful investigation of the combination of the various vortex models has shown that the use of a potential vortex together with a Rosenhead vortex will indeed represent the measured velocity profile with sufficient accuracy.

The use of Eqs. (2) and (6) yielded,

$$\frac{v}{v_o} = \frac{X\Sigma^2}{\left[X^2\Sigma^2 + (1-H)^2 + \Sigma^2\right]} - \frac{X\Sigma^2}{\left[X^2\Sigma^2 + (1+H)^2 + \Sigma^2\right]}$$

$$+ \frac{1}{2}\left[\frac{X\Sigma^2}{\left[X^2\Sigma^2 + (1-H)^2\right]} - \frac{X\Sigma^2}{\left[X^2\Sigma^2 + (1+H)^2\right]}\right] \qquad (13)$$

The comparison of the measured velocities (v component only) with those calculated through the use of Eqs. (12) and (13) will be made in the course of the discussion of results.

IV. EXPERIMENTAL EQUIPMENT

Experiments were conducted in a low turbulence water tunnel with an open test section 38 cm wide, 50 cm deep (maximum), and 130 cm long. The turbulence management system was located upstream of the test section. It consisted of a honeycomb and fine-mesh screen (see Figure 2). The tunnel was driven by a 50 Hp centrifugal pump. A second but smaller pump continuously circulated the tunnel water through a micro filtration system to remove any suspended fine particles from the tunnel water (the filtration system was turned off during the experiments).

A vertically mounted rectangular foil (NACA 0008) was used to generate 'single' vortices shedding from the free end of the foil. The tip of the wing was rounded to a radius equal to half the local thickness of the foil. The interior of the model was hollowed and connected to a dye reservoir to seed the vortex core with a fluorescent dye. The chord length, c, of the foil was 87 mm. The distance from the test section floor (plane of reflection) to the top of the tip was varied from 46 cm to 48 cm resulting in aspect ratios ranging from 10.6 to about 11. The leading edge of the foil was 3.6 chord lengths downstream of the test section entrance. The chord-based Reynolds number was 43,500.

The foil was mounted in a rotatable cylindrical base, embedded into the bottom of the test-section floor. Its height and angle of attack were set at the desired values, while the water level was held constant. For models with large aspect ratios, the small change in aspect ratio, as the model tip

approached the free surface, does not significantly change the circulation of the vortex and, hence, the vortex/free-surface interaction.

The angle of attack was held at 12 degrees. The measurements were taken at a section 3.6 chord lengths downstream of the trailing edge. The total circulation of the fully-submerged trailing vortex was calculated from the tangential velocity distribution and from (Durand, 1963)

$$\Gamma/Uc = [1.05\pi(\alpha - \alpha_o)]/(1 + 2/AR)$$

including a correction for the wall effect of the tunnel floor. The normalized vortex strength, Γ/Uc, was 0.025 m^2/s (0.018 m^2/s of this circulation was within the 12 mm core and 0.007 m^2/s was outside the core). The calculated values were within a few percent of those obtained from the tangential velocity distribution. This was considered to be sufficiently accurate considering the fact that the determination of the strength of a tip vortex is no simple matter.

The velocities and turbulence intensities were measured with a Laser-Doppler Anemometer. The primary result of a laser anemometer measurement is a current pulse from the photodetector. this current contains the frequency information relating to the velocity to be measured. The quality of the signal and the performance of the signal processor are dependent on the number of seeding particles present simultaneously in the measuring volume. In the present investigation particles of less than 10 micron diameter were used to seed the tunnel. The velocity information obtained from the Doppler signal as a frequency modulation of the detector

current was processed electronically through the use of a commercially available software.

Initial measurements were dedicated to the establishment of the tunnel characteristics at the section. The measurements have shown that the velocity was uniform (except in the boundary layers, of course) within 1%, in both the vertical and horizontal directions. The freestream turbulence intensity was not isotropic but the maximum value did not exceed 0.1%.

V. DISCUSSION OF RESULTS

A. INTRODUCTION

First the velocities and then the turbulence intensities are discussed. The presentation of the velocities is, in turn, divided into two parts:

(i) The discussion of the v-component of velocity for a deeply-submerged foil ($h_o/\sigma_o = 8.3$) and for a foil with shallower depth ($h_o/\sigma_o = 3.85$). These are compared, whenever appropriate, with the theoretical predictions; and

(ii) The discussion of the u-component of velocity for both the shallow and deeply-submerged foils. Subsequently, the discussion of the turbulence intensities are undertaken, following the aforementioned order of presentation.

B. DISCUSSION OF THE V-COMPONENT OF VELOCITY

Figure 3 shows the v-component of velocity, resulting from the Rosenhead model, for $h_1/h_o = 1$, 0.8, 0.4, and 0.2 (all for $h_o/\sigma_o = 8.3$). Three facts are self evident: The velocity profile is symmetric, save for the sign of velocity, the core radius increases with decreasing h_1/h_o, and the maximum velocity decreases at a rate faster than the decrease in depth.

Figures 4 through 7 show the experimental data and the idealized velocity profiles of Rosenhead for $h_1/h_o = 1$, 0.8, 0.4, and 0.2, respectively, all for $h_o/\sigma_o = 8.3$. It appears that the Rosenhead profile faithfully represents the data practically for all values of X/R_o. The slight difference between the two

profiles near $X/R_o = 4$ may be due to the effect of the free surface on the part of velocity where the gradients are relatively sharp. Even though there are two such regions on the profile, the asymmetry in the measured profile occurs only near $X/R_o = 4$, not near $X/R_o = -4$. The reason for this may be due to the fact that the motion of the vortex in Figs. 4–7 is counter-clockwise and the fluid is pushed upwards for $X/R_o > 0$, and downwards for $X/R_o < 0$. Thus the free surface deformations or vertical swelling is on the right side of the figure, i.e., for $X/R_o > 0$. This effect is accentuated in horizontal planes closer to the free surface, i.e., for smaller values of h_1/h_o, as seen in Figs. 5-7. In examining the relative magnitudes of measured and predicted velocity profiles one must bear in mind the fact that the idealized profile assumes a rigid surface and the Rosenhead model is not an exact solution of the Navier-Stokes equations, let alone the solution for two such vortices across a non-deformable surface. Nevertheless, the measured v-components of velocity exceeding those calculated for $X/R_o > 0$ and vice versa for $X/R_o < 0$ is not entirely unexpected. For the Rosenhead profile, the rigid boundary (free surface) inhibits the upward motion or swelling of the fluid so as to satisfy the 'no-penetration' condition. For the real fluid motion, however, the fluid can and does move upwards, symbolizing the presence of surface sinks, in addition to image vortices. These are naturally expected to yield larger v-components in the upward direction and lower v-components in the downward direction.

The simulations and data similar to those presented in Figs. 3–7 are shown in Figs. 8 through 14 for $h_o/\sigma_o = 3.85$ and for various values of h_1/h_o. Figure 8 shows the Rosenhead profiles for $h_1/h_o = 1.6$, 1.0, 0.80, 0.6, 0.4, and 0.36. As noted before, the v-component of the velocity decays rapidly as one

approaches the free surface. This is an expected consequence of the boundary conditions imposed on the simulation. The data shown in Fig. 9 are rather unusual in the sense that it is for a horizontal plane below the trailing vortex. Thus, one would expect nearly perfect agreement between the measured and calculated values for such a deeply-submerged plane. The fact that it is not so is evident from the said figure, particularly for $X/R_o > 6$. This is thought to be due to the wake of the foil. It is recalled that for $h_1/h_o = 1.6$, the level at which the measurements are made, is below the tip of the foil. Considering the fact that the vorticity shed from the foil does not fully roll-up into the tip vortices within a downstream distance of $x/c = 3.6$, where the measurements are made, one would expect to see the effect of the remaining vorticity on the velocity profile. The calculations, not shown here, predicted that the effect of the remaining vorticity will manifest itself at about $X/R_o > 6$.

Figures 10 and 11, representing data at $h_1/h_o = 1.0$ and 0.80, show that the wake effect has disappeared and the measured profiles agree more closely with those predicted by the Rosenhead model. Figures 12–14 show, as discussed previously, the increasing effect of the free-surface proximity and the evolution of asymmetry in the velocity profile. Even though the vortex core grows with decreasing depth even for a non-deforming free surface, as in the case of the Rosenhead profiles, the effect of the deformation of the free surface further enhances the core growth as seen in Figs. 13 and 14.

C. DISCUSSION OF THE U-COMPONENT OF VELOCITY

The axial velocity defect is shown as a function of X/R_o in Figs. 15 through 17 for $h_o/\sigma_o = 8.3$ and in Figs. 18 through 21 for $h_o/\sigma_o = 3.85$. Clearly, the axial velocity near the vortex core (Fig. 15) is smaller than that in the ambient flow. Even though there has been considerable debate in the past regarding the direction of the axial velocity (see, e.g., Singh and Uberoi, 1976), it is generally agreed that there is a velocity defect and not a velocity excess in planes at relatively small distances downstream from the foil. The effect of this defect in planes further away from the vortex core decreases rapidly as seen in Figs. 16 and 17. However, it is rather noteworthy that the effect of the free-surface proximity is to make the defect asymmetrical (Figs. 16-17). In the region even closer to the free surface (Fig. 17), where the free surface moves upwards ($X/R_o > 0$), the velocity defect almost disappears.

The velocity defect for the case of $h_o/\sigma_o = 3.85$ is shown in Figs. 18 through 21. Figure 18 is particularly interesting for it exhibits simultaneously the effect of nearly symmetrical velocity defect (at least for $X/R_o < 4$) and the effect of the foil wake (near $X/R_o = 7$), as it would be expected in a plane at a relatively large depth ($h_1/h_o = 1.6$). It is equally interesting to note that had there been no wake effect, the velocity defect profile could have smoothly joined between $X/R_o = 4$ and $X/R_o = 16$, as seen in Fig. 18. In fact, Fig. 19 shows that for $h_1/h_o = 1$ the wake effect disappears and the velocity defect profile becomes nearly symmetrical. For planes closer to the free surface, Figs. 20 and 21 show that the velocity defect becomes once again asymmetrical. Furthermore, a comparison of Figs. 17 (for $h_o/\sigma_o = 8.3$ and $h_1/h_o = 0.2$) and 21

(for $h_o/\sigma_o = 3.85$ and $h_1/h_o = 0.4$) show that they become nearly identical regardless of the depth at which the trailing vortex is generated.

D. DISCUSSION OF TURBULENCE COMPONENTS

The turbulence intensity Tu ($= \sqrt{\overline{v'^2}} / V_o$ = Root-Mean-Square value of the v'-component of turbulence normalized by V_o, the maximum velocity in the trailing vortex), is shown as a function of X/R_o in Figs. 22 through 25 for $h_o/\sigma_o = 8.3$ and in Figs. 26 through 31 for $h_o/\sigma_o = 3.85$.

According to Figs. 22 and 23, the turbulence intensity near the vortex core is rather high relative to that at the outer edges of the vortex. There has been considerable debate as to whether this is genuine turbulence or whether it is a manifestation of the wandering of the vortex core. There has been further debate regarding the origin of the vortex wandering, observed in almost every wind- and water-tunnel. It has often been assumed that the large axial velocity fluctuations near the core may be caused primarily by the random motion or wandering of the trailing vortex about the measurement point in a region where the velocity gradients are very large. Obviously, very small motions in such a field produce large pseudo velocity fluctuations, i.e., the measurements reflect both temporal and spatial unsteadiness. Recently, Sarpkaya (1992) has shown that numerous tentacle-like vortex sheets of finite length, resulting from helical instabilities, stretch out or are thrown away from the outer edges of the vortex core. The vortex peels off randomly and sheds vorticity along its length. The core of a turbulent vortex is not a benign, smooth, axisymmetric, solid body of rotation. The exchange of momentum

between the outer regions and the core leads to the oscillation of the vortex core and the various velocity components. The evolution of the momentum exchange and the unsteadiness in various velocity components that result from it must certainly depend on the characteristics of the foil, transition in its boundary layers, Reynolds number, ambient turbulence, and the mutual interaction of the trailing vortices with each other or with their images across a deformable or rigid boundary. It is not the purpose of the present investigation to repeat some of the previous works which have dealt with the trailing vortices in an effectively infinite medium (Sarpkaya, 1983; Green & Acosta, 1991), but rather, to present evidence that the turbulent vortex core is neither axisymmetric nor smooth and that the interaction of such a vortex with the free surface leads to scars.

Figures 24 and 25 show that the turbulence intensity decreases in planes closer to the free surface. Normally, one would assume that this should be so and that the vertical velocity and turbulence fluctuations must go to zero as a consequence of the plane free surface boundary. However, the interaction of the vortex with the free surface gives rise to considerable surface signatures (scars and whirls with vertical axes), and the vertical fluctuations need not go to zero as the surface is approached. Nevertheless, one would expect diminishing turbulence intensities, with finite terminal values, as the free surface is approached, as seen in Figs. 24 and 25.

Figures 26 through 31 show the turbulence intensity for $h_o/\sigma_o = 3.85$ for $h_1/h_o = 1.6$, 1, 0.80, 0.60, 0.40, and 0.36. The interesting observations are that (i) in a plane below the vortex, ($h_1/h_o = 1.6$), the turbulence distribution is fairly symmetric and the effect of the wake (near $X/R_o = 7$), even though clearly

manifested, is relatively small. At the level of the vortex, ($h_1/h_o = 1$), the region near the vortex core exhibits, once again, large turbulence intensities. As noted earlier, this may be attributed to vortex wandering resulting from the peeling off of the vortex sheets and the ambient turbulence. In general, turbulence intensities do not exhibit large variations until one comes very close to the free surface. In fact, a comparison of the Figs. 30 and 31 shows that almost suddenly, the turbulence intensity in the vertical direction begins to decrease. During the current experiments it was not possible to make measurements at distances closer than $h_1/h_o = 0.36$. Additional attempts will be made in the near future to remedy this situation since the importance of making measurements at even closer distances has been clearly demonstrated.

Figures 32 through 38 deal with turbulence in the direction of the free stream, i.e., in the axial direction as far as the vortex motion is concerned. Also plotted in these figures is the corresponding velocity defect. The reason for this is the expectation that there might be some correlation between the turbulence intensity and the velocity defect. Here the turbulence intensity, denoted again by the same symbol Tu, is defined as the ratio of the Root-Mean-Square value of the u' fluctuations to the ambient velocity U_o, i.e., $Tu = \sqrt{\overline{u'^2}}/U_o$. It should also be noted that in Figs. 32–38, **five times** the turbulence intensity is plotted in order to separate it from the velocity defect data.

Apparently, slightly away from the vortex core, the turbulence becomes more or less uniform across the section but does not show any significant increase or decrease. Normally, one would have expected a conversion of the vertical component of the turbulence energy into horizontal components.

Apparently, the deformation of the free surface makes such expectations too simplistic. Additional measurements are necessary for a better understanding of the reasons and in particular for the exploration of the possibility that even though the vertical components decrease and the axial components remain relatively unchanged, the lateral components may increase significantly. Such measurements will be undertaken in the very near future as part of the on-going investigation.

Figures 35 through 38 show, once again, **five times** Tu ($= \sqrt{\overline{u'^2}}/U_o$) for $h_o/\sigma_o = 3.85$ and the corresponding velocity defects. In the plane below the vortex (Fig. 35), Tu is nearly uniform. In the plane passing through the vortex (Fig. 36), Tu increases near the core and is affected by the proximity of the free surface for $X/R_o > 4$. The axial turbulence is still considerably large near the vortex axis even at distances as small as $h_1/h_o = 0.8$ as seen in Fig. 37. However, at $h_1/h_o = 0.4$ (Fig. 38), Tu decreases sharply and becomes nearly uniform. This is more in line with the expectations noted earlier and in complete agreement with the observations of Sarpkaya and Henderson (1985) and Sarpkaya (1985) that the striations come into existence when the vortex is at a distance of about one core radius from the free surface (in the present case, $h_1/\sigma_o = 1.39$). These results point out, once again, the fact that the most important fluctuations, conversion of turbulence energies, and scars and striations occur at or very near the free surface.

VI. CONCLUSIONS

The interaction of a single turbulent trailing vortex has been investigated through the use of an LDV system for the purpose of exploring the origins of scars, striations, and three-dimensional instabilities. The evidence presented herein shows that the vertical component of the velocity is affected by the wake of the foil (if the plane of measurement is below the wing tip), by the proximity of the free surface, and more importantly, by the deformation of the free surface. In fact the asymmetrical deformations of the free surface render the velocity distributions equally asymmetrical.

The axial velocity shows a defect in almost all planes. However, the velocity defect near the free surface diminishes to a finite value. Both the vertical and axial turbulence intensities are large near the vortex core. However, particularly the results obtained with a trailing vortex near the free surface show that the vertical component of turbulence decreases rapidly very near the free surface. This is in conformity with the earlier observations that scars and striations are generated only when the vortex is at about one or two core radii from the free surface.

The idealized representations of the velocity profiles through the use of the Rosenhead and potential flow models have shown that the measurements at or near the vortex core can be faithfully represented by the said models. However, further away from the core, and in particular near the free surface, the deformation of the free surface and not the 'no penetration' condition dominates the velocity distribution. Thus, the measured and calculated values differ increasingly as one approaches the free surface. The

differences are both informative and indicative of the role played by the free surface.

The use of a turbulent vortex (and its image) near the free surface of an otherwise smooth uniform flow proved to be a 'kernel' experiment towards the elucidation of the dynamical processes in vorticity/free-surface interaction which can be studied in isolation, without complications and competing influences that normally occur in a fully turbulent ship wake. The results have shown unmistakably that the most important free surface signature events take place near the free surface. It is because of this reason that detailed velocity and turbulence measurements at other Reynolds numbers and foil conditions are needed to delineate the characteristics of the scars and striations.

APPENDIX

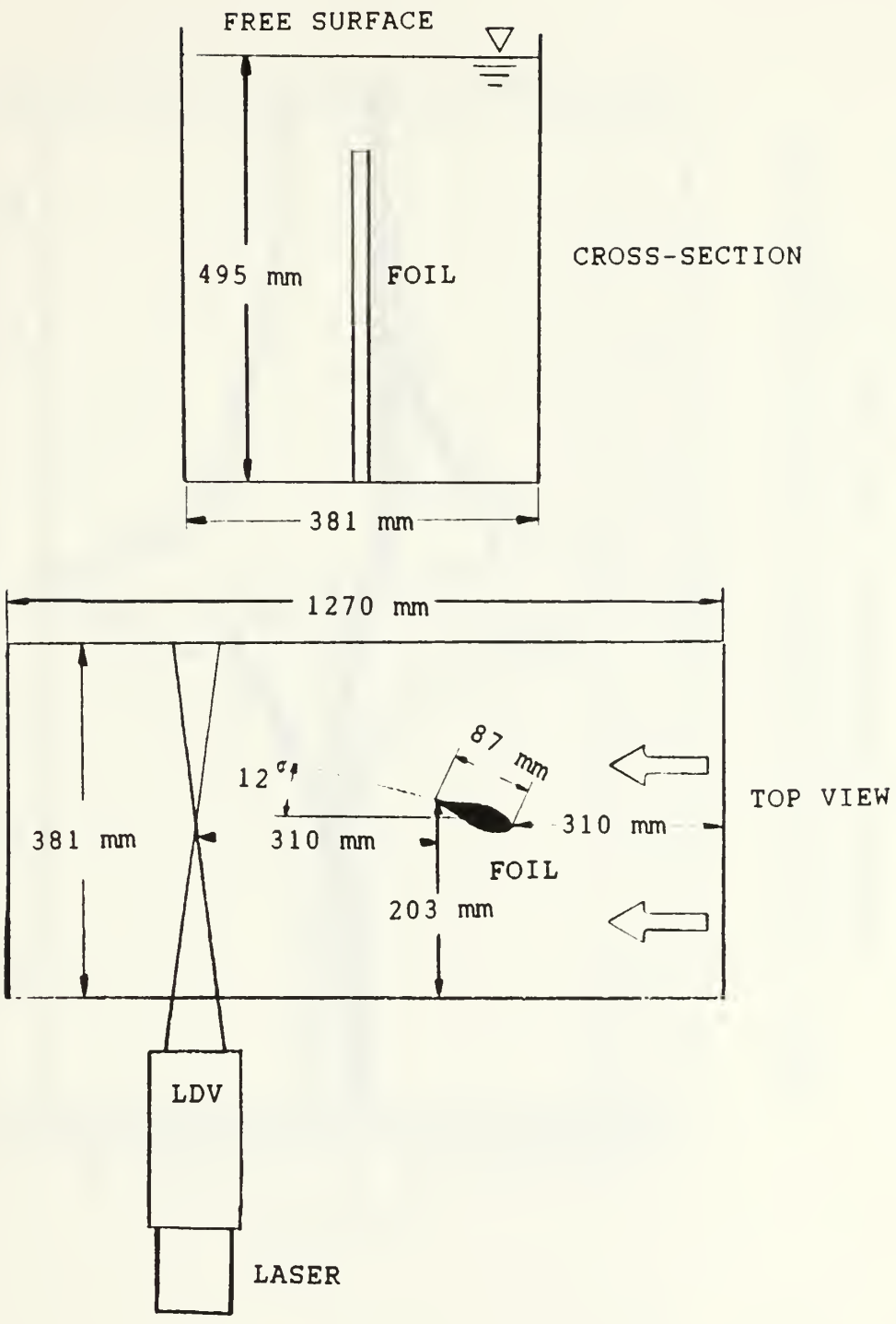

Figure 2. Schematic Drawing of the Test Section

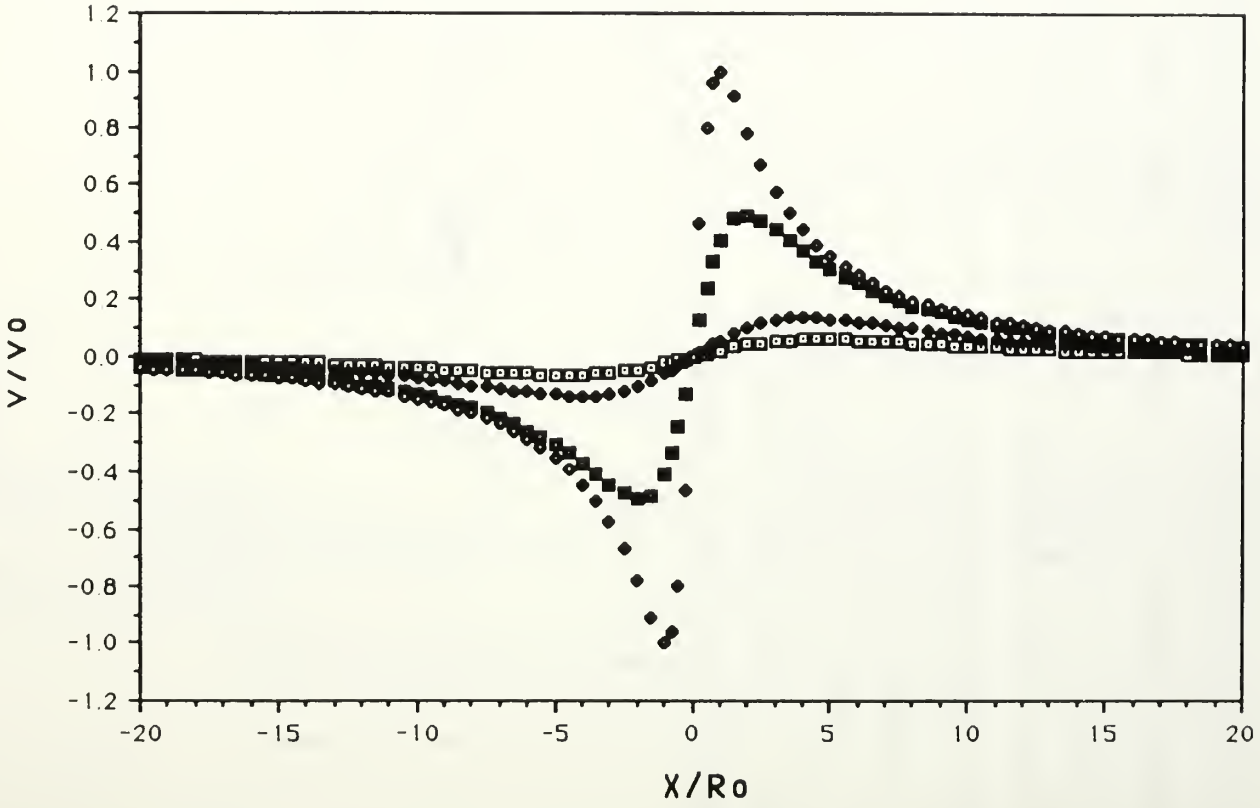

Figure 3. Composite Plot of Rosenhead Profiles versus Radial Distance

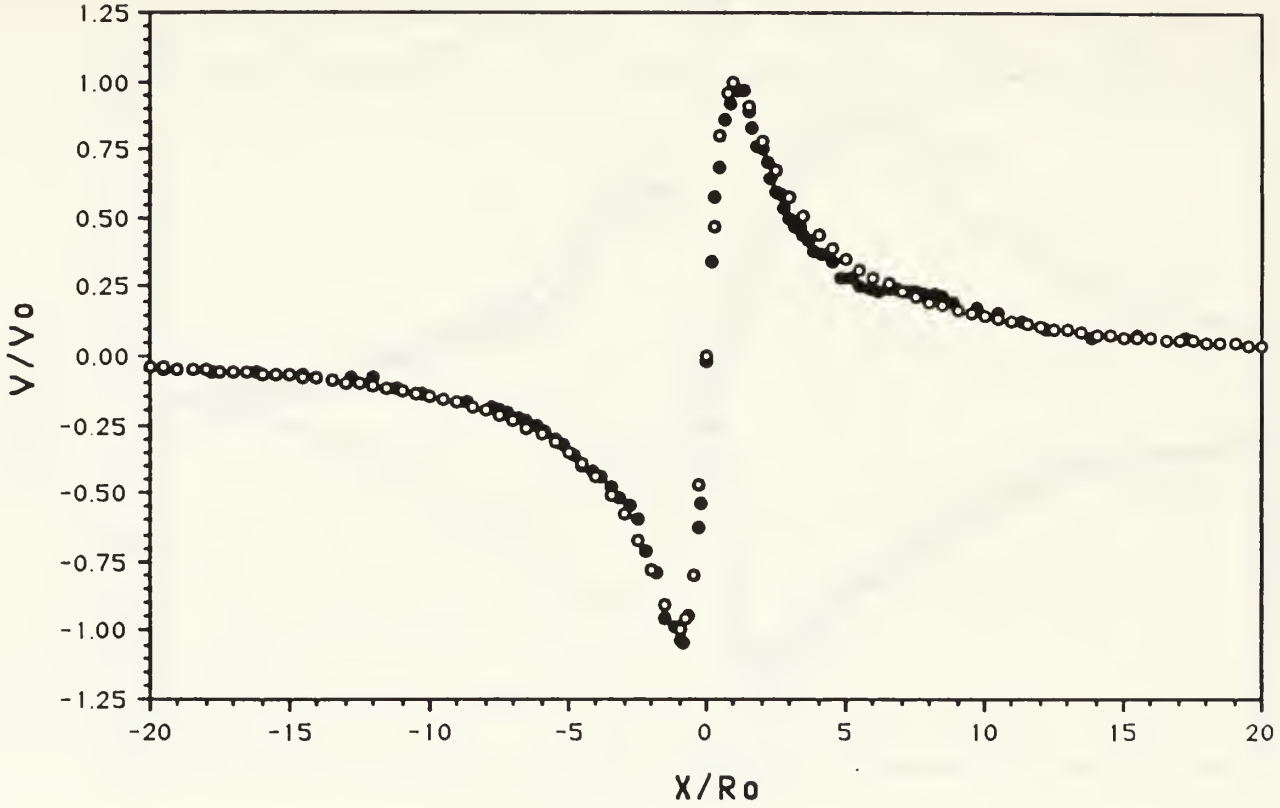

Figure 4. Comparison of the Measured v-component of Velocity with Rosenhead Profile for $h_1/h_o = 1.0$ and $h_o/\sigma_o = 8.3$

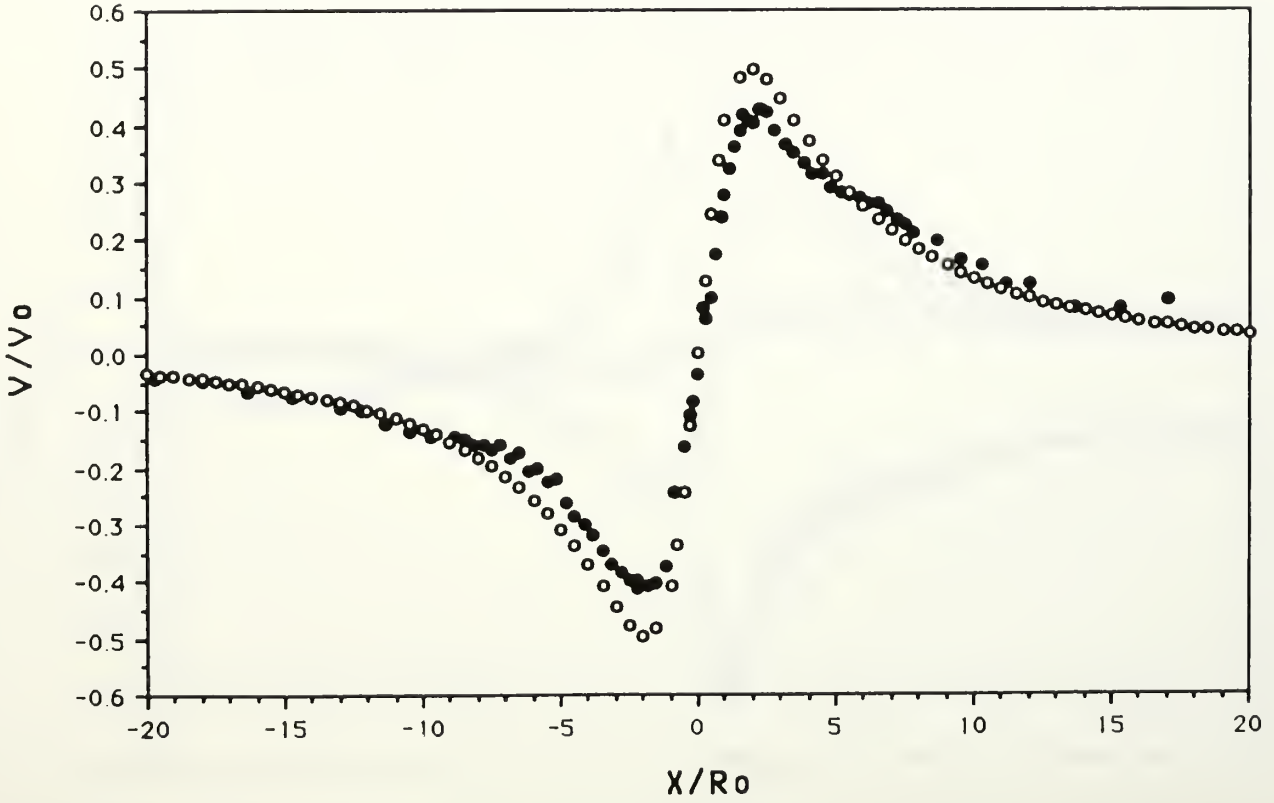

Figure 5. Comparison of the Measured v-component of Velocity with Rosenhead Profile for $h_1/h_o = 0.8$ and $h_o/\sigma_o = 8.3$

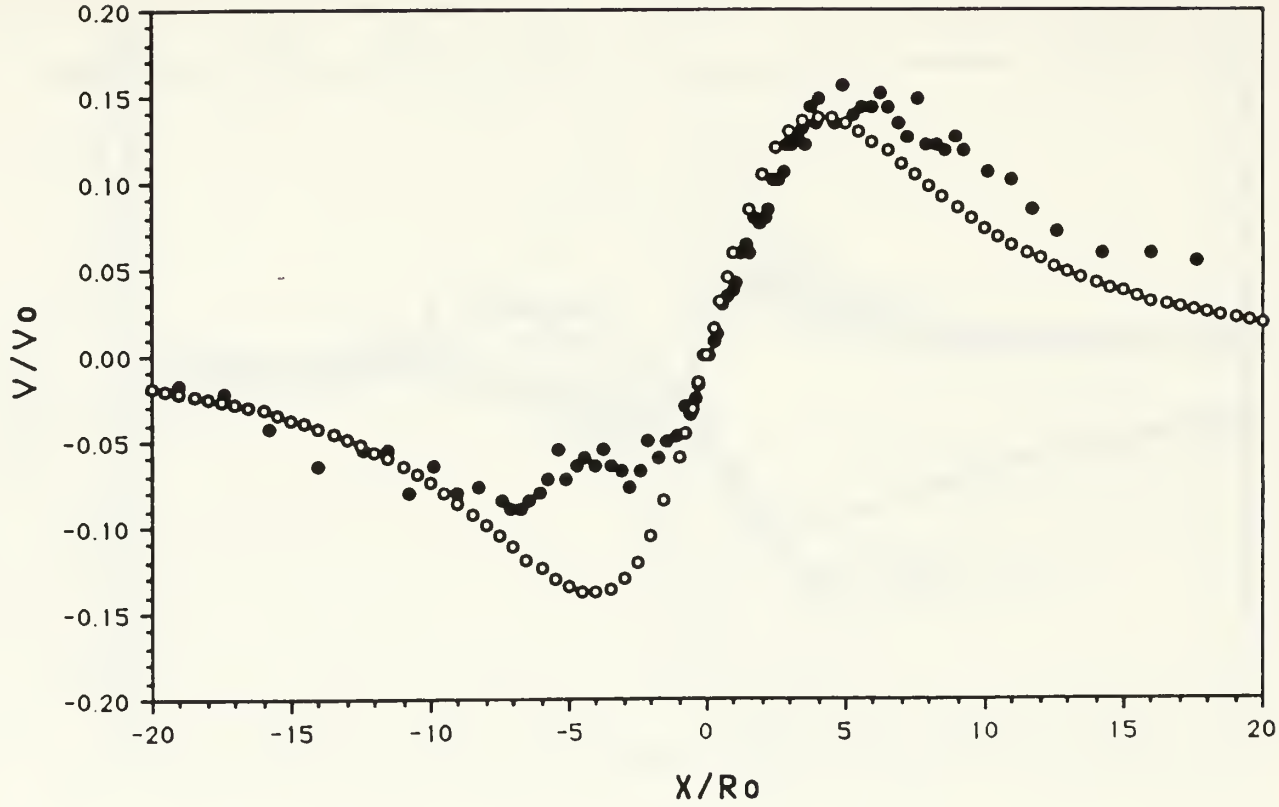

Figure 6. Comparison of the Measured v-component of Velocity with Rosenhead Profile for $h_1/h_o = 0.4$ and $h_o/\sigma_o = 8.3$

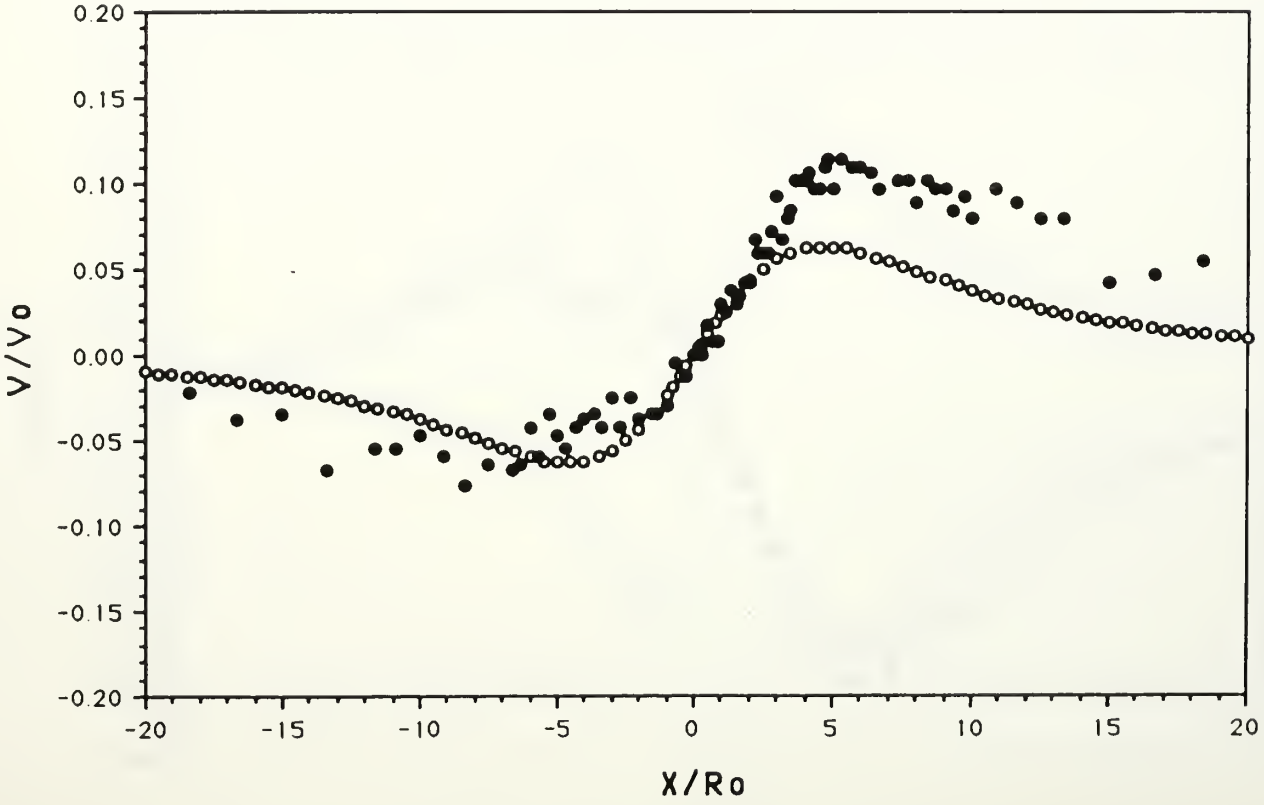

Figure 7. Comparison of the Measured v-component of Velocity with Rosenhead Profile for $h_1/h_o = 0.2$ and $h_o/\sigma_o = 8.3$

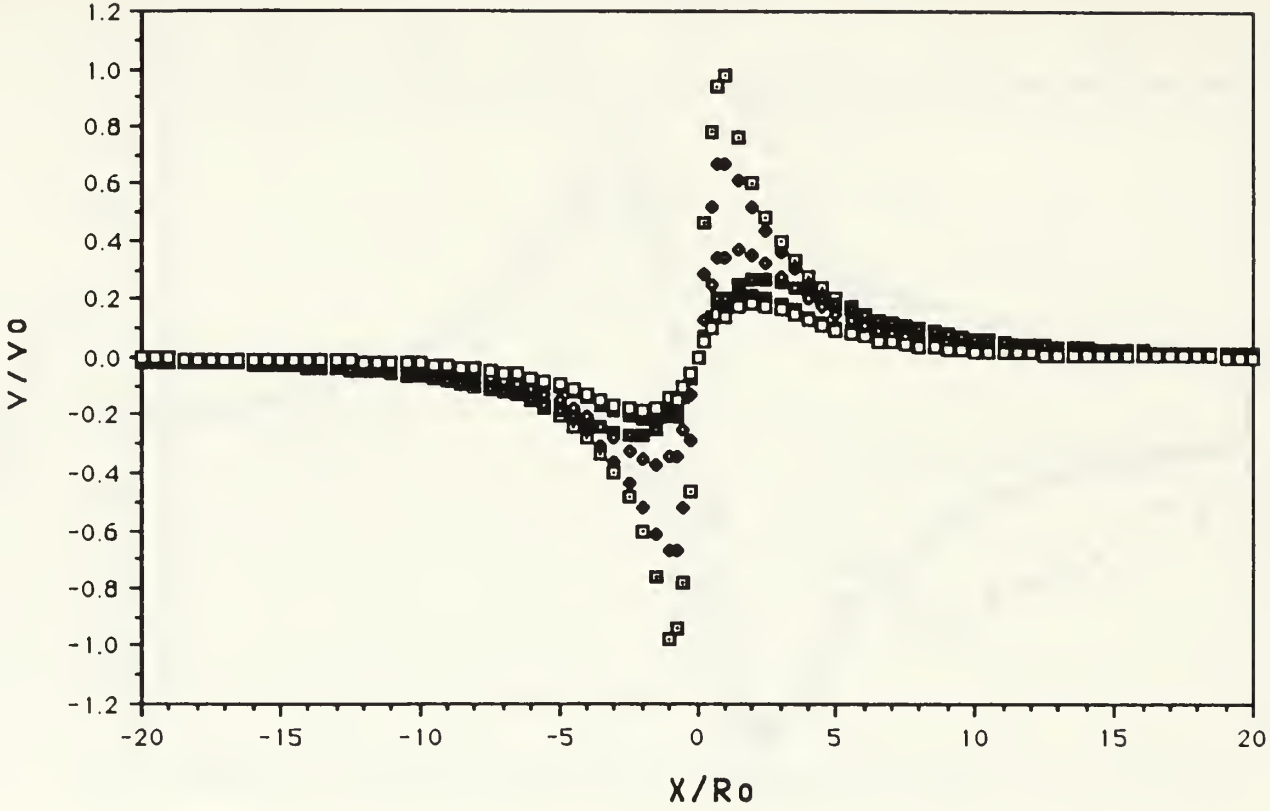

Figure 8. Composite Plot of Modified Rosenhead Profiles versus Radial Distance

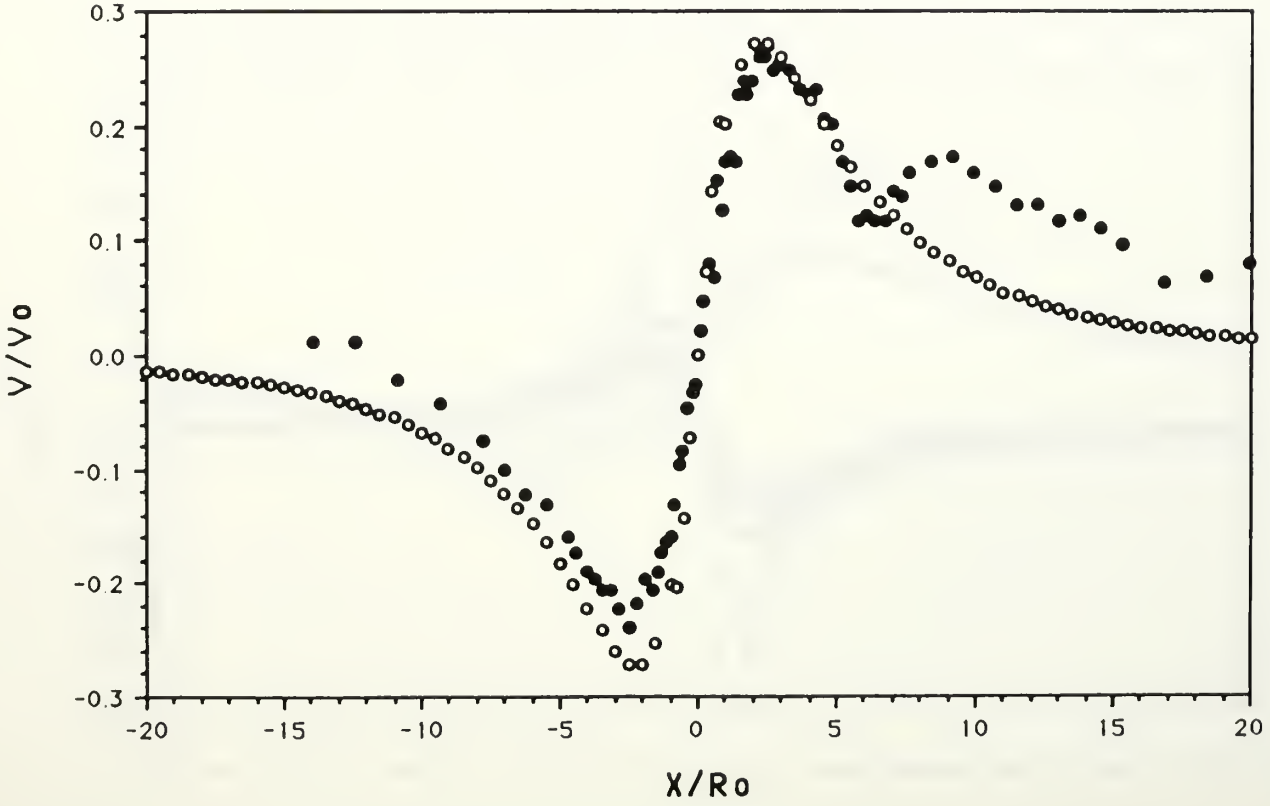

Figure 9. Comparison of the Measured v-component of Velocity with Rosenhead Profile for $h_1/h_o = 1.6$ and $h_o/\sigma_o = 3.85$

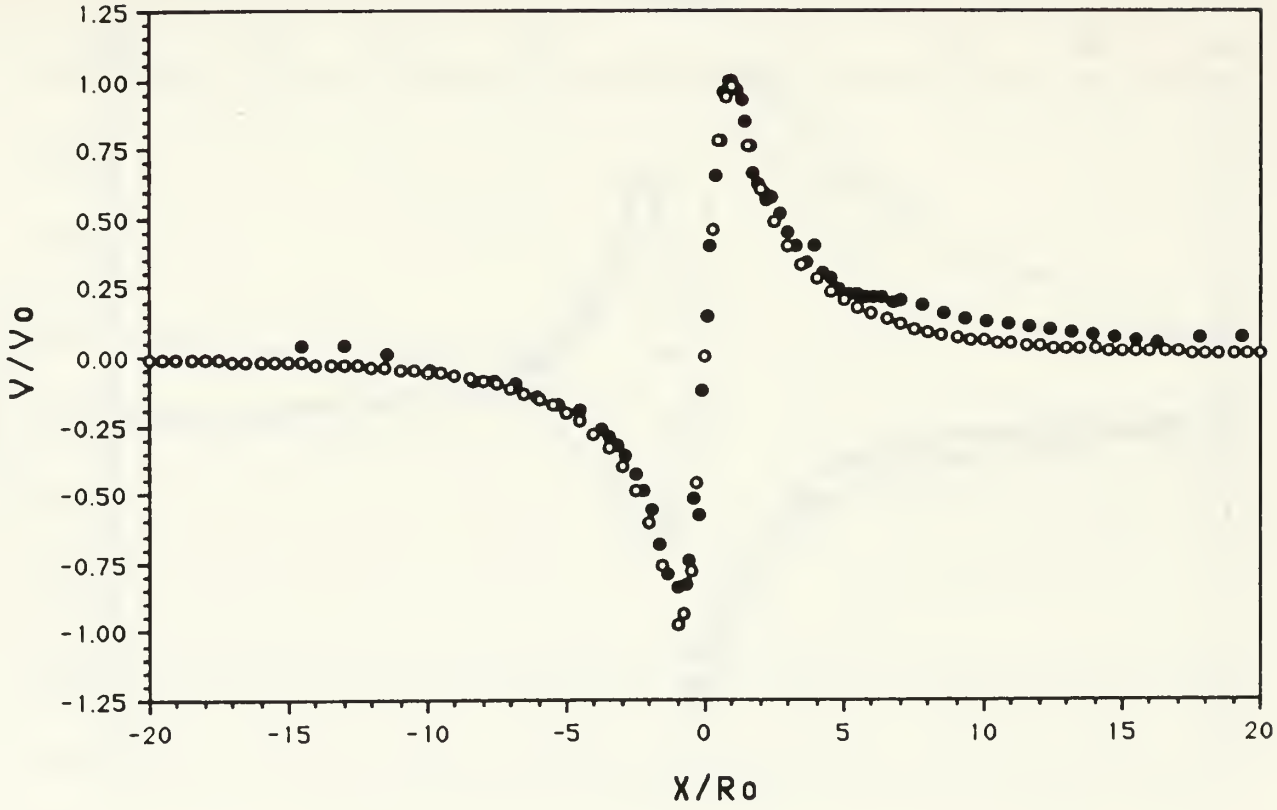

Figure 10. Comparison of the Measured v-component of Velocity with Rosenhead Profile for $h_1/h_o = 1.0$ and $h_o/\sigma_o = 3.85$

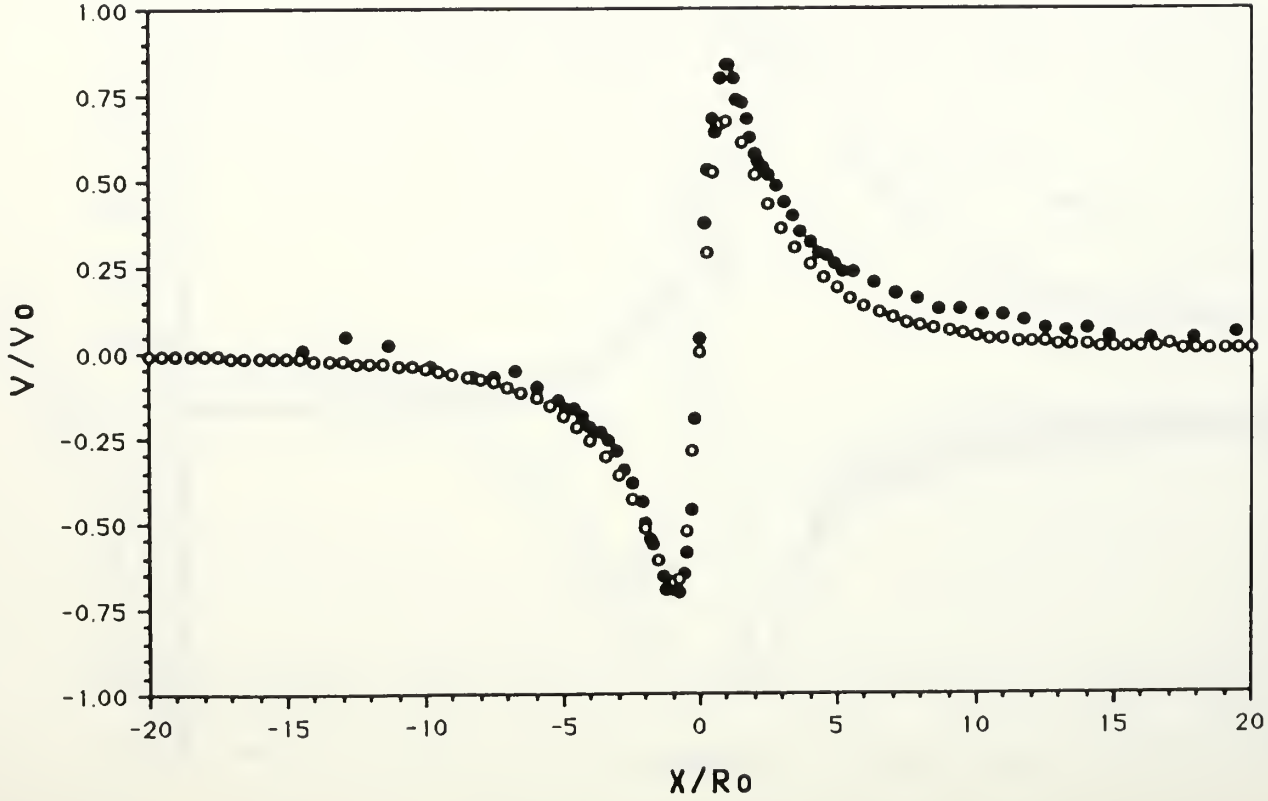

Figure 11. Comparison of the Measured v-component of Velocity with Rosenhead Profile for $h_1/h_o = 0.8$ and $h_o/\sigma_o = 3.85$

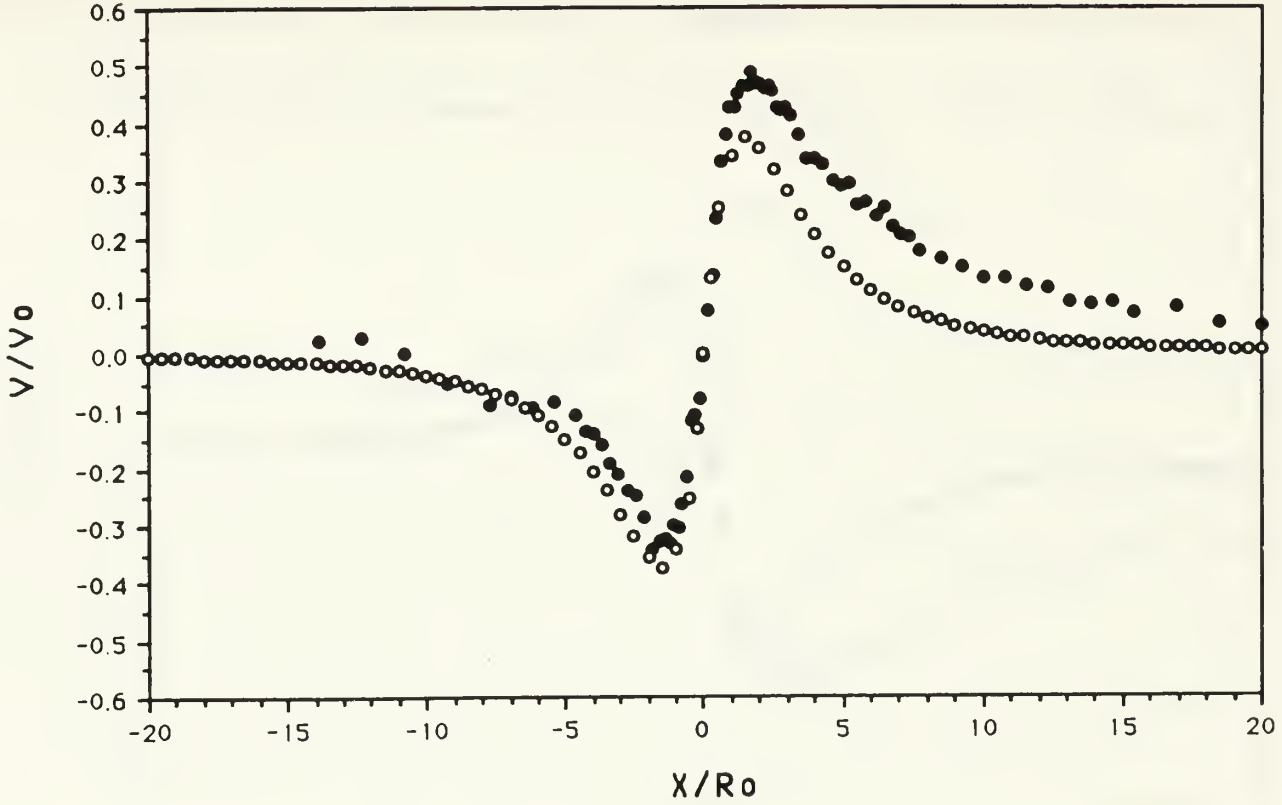

Figure 12. Comparison of the Measured v-component of Velocity with Rosenhead Profile for $h_1/h_o = 0.6$ and $h_o/\sigma_o = 3.85$

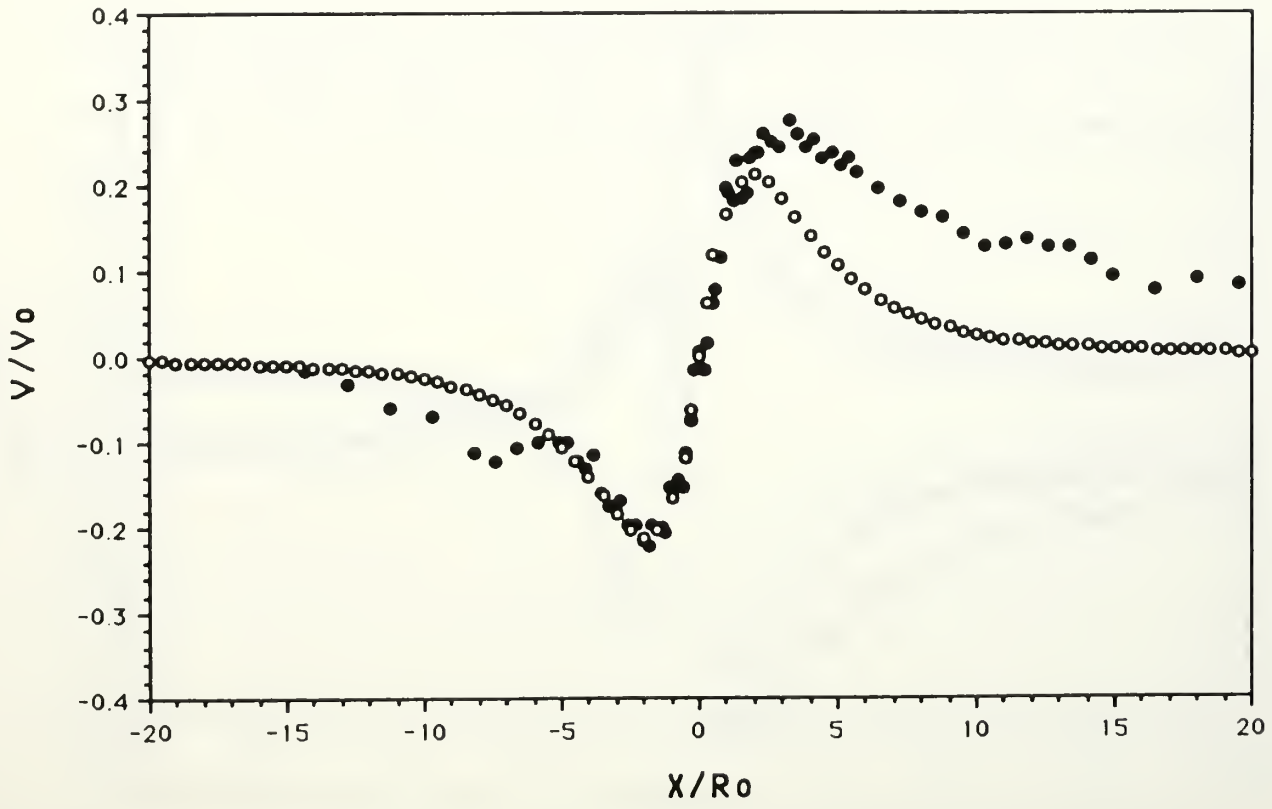

Figure 13. Comparison of the Measured v-component of Velocity with Rosenhead Profile for $h_1/h_o = 0.4$ and $h_o/\sigma_o = 3.85$

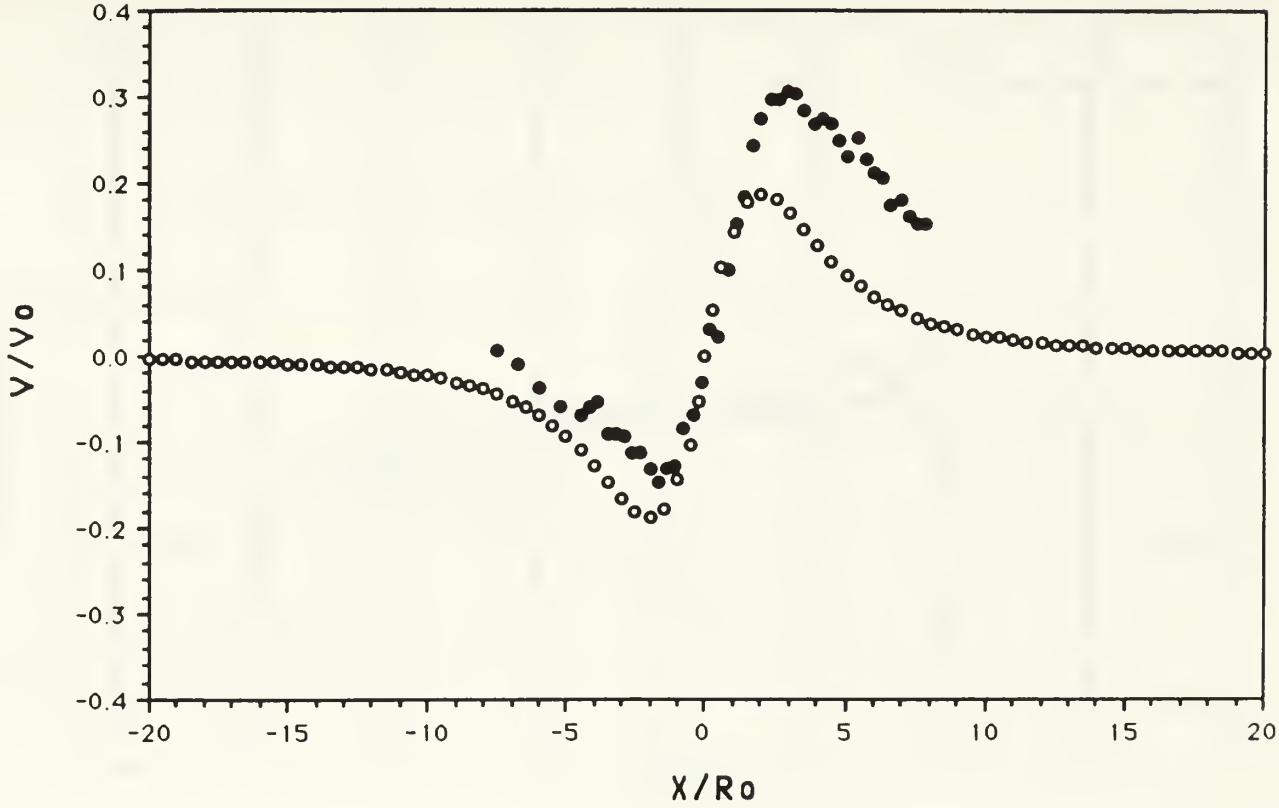

Figure 14. Comparison of the Measured v-component of Velocity with Rosenhead Profile for $h_1/h_o = 0.36$ and $h_o/\sigma_o = 3.85$

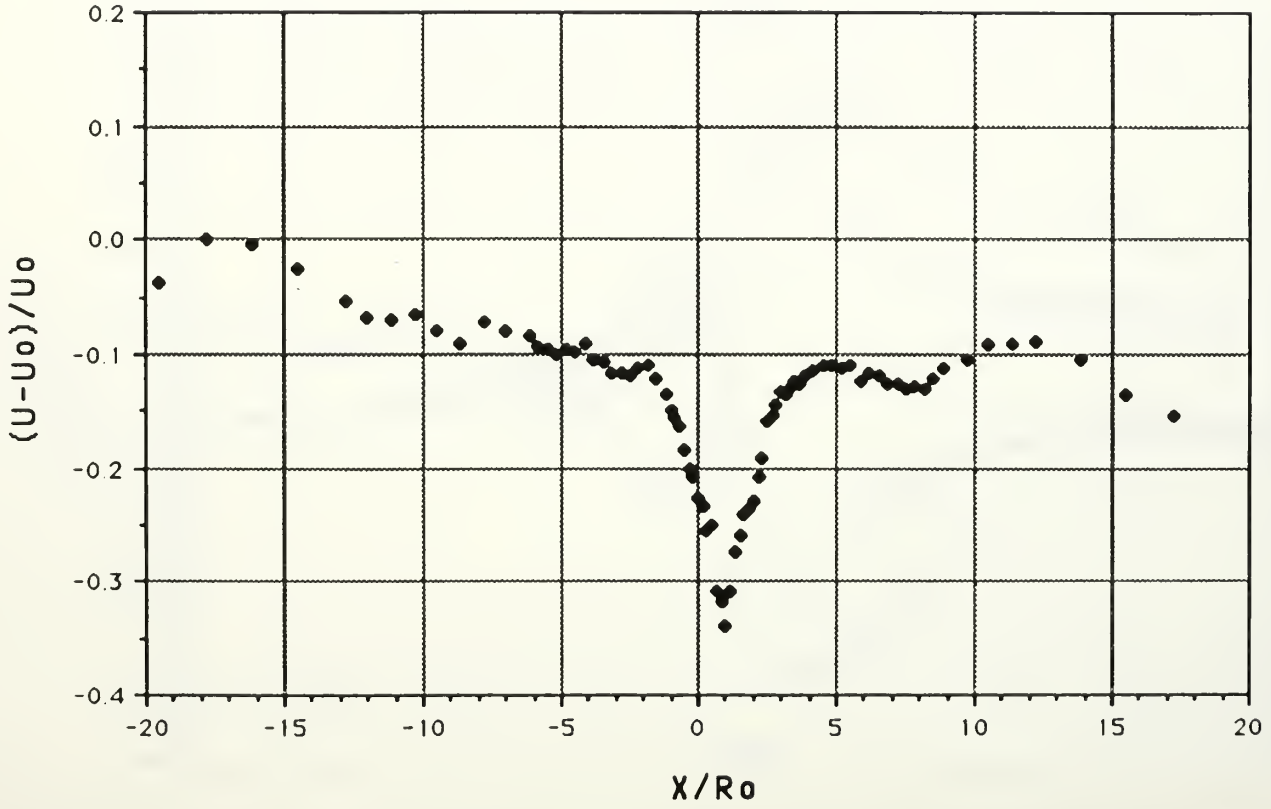

Figure 15. Axial Velocity Defect versus Radial Distance for $h_1/h_o = 1.0$ and $h_o/\sigma_o = 8.3$

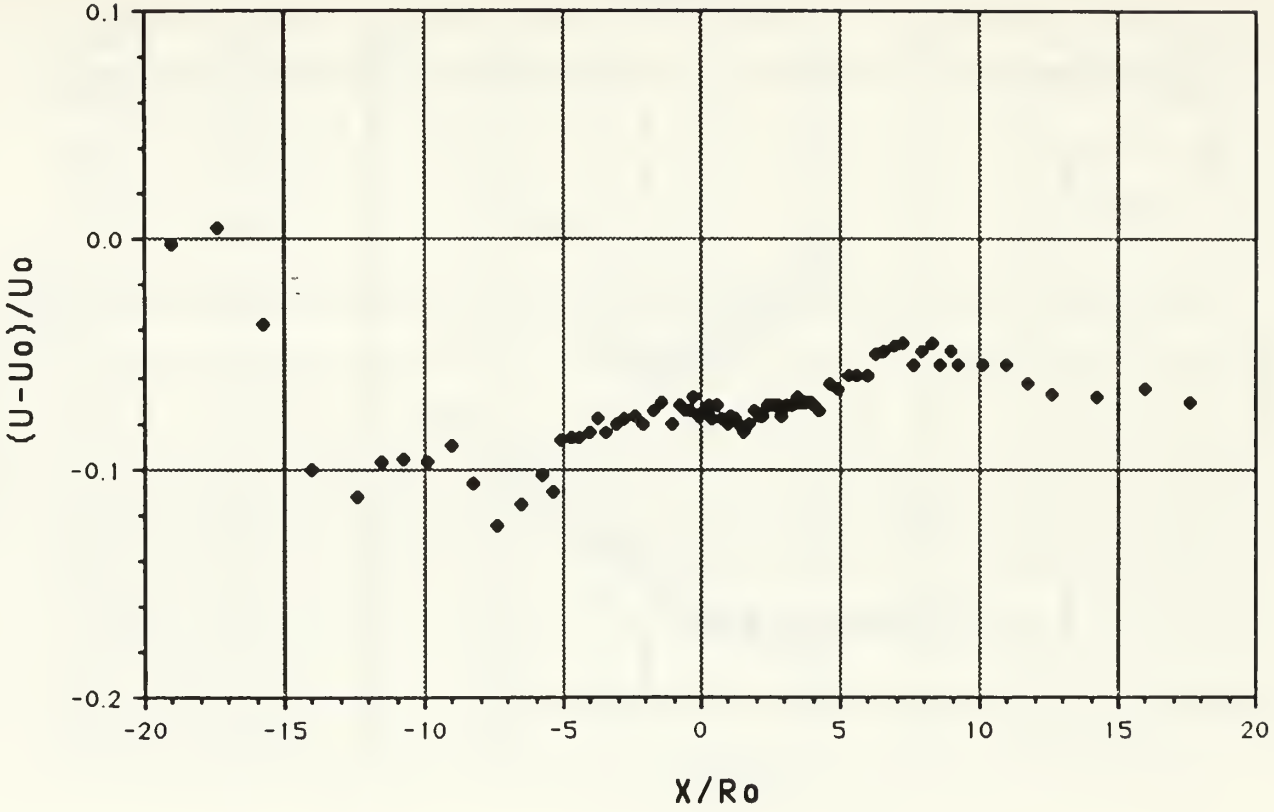

Figure 16. Axial Velocity Defect versus Radial Distance for $h_1/h_o = 0.4$ and $h_1/\sigma_o = 8.3$

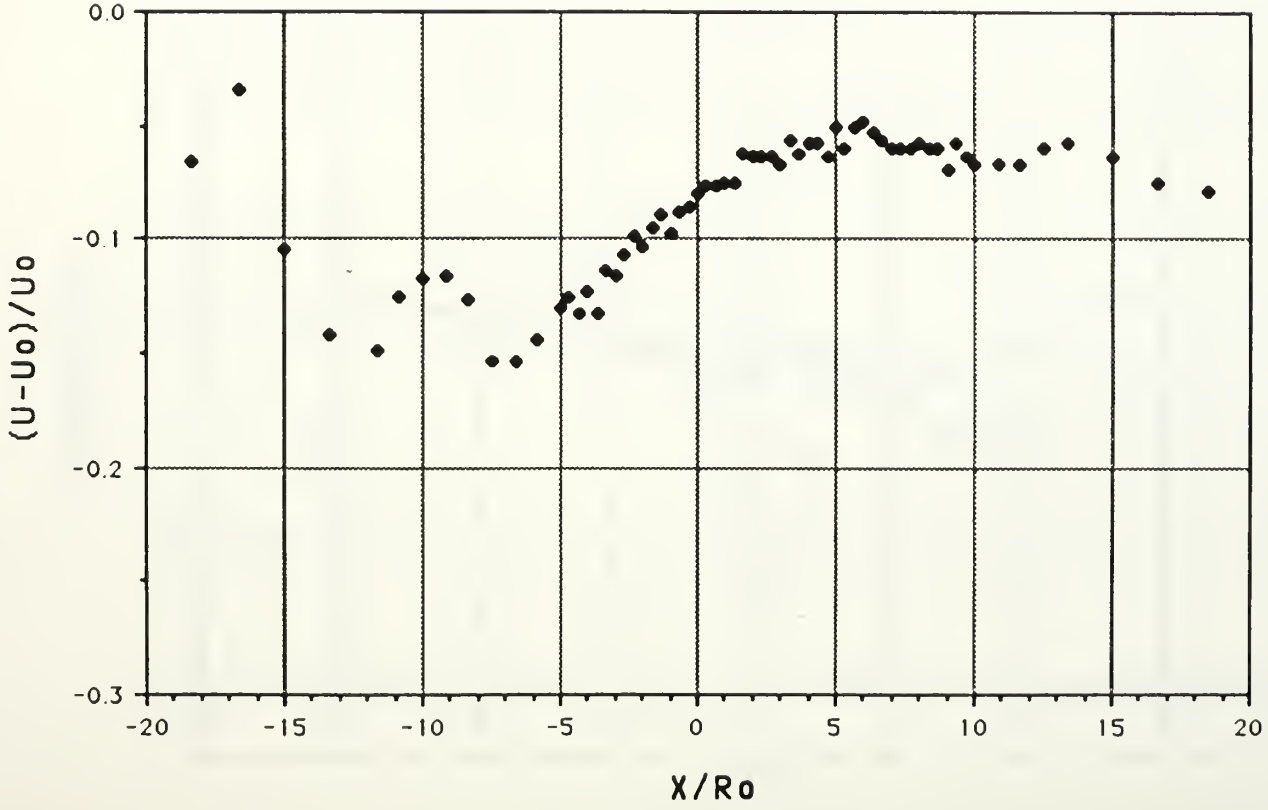

Figure 17. Axial Velocity Defect versus Radial Distance for $h_1/h_o = 0.2$ and $h_o/\sigma_o = 8.3$

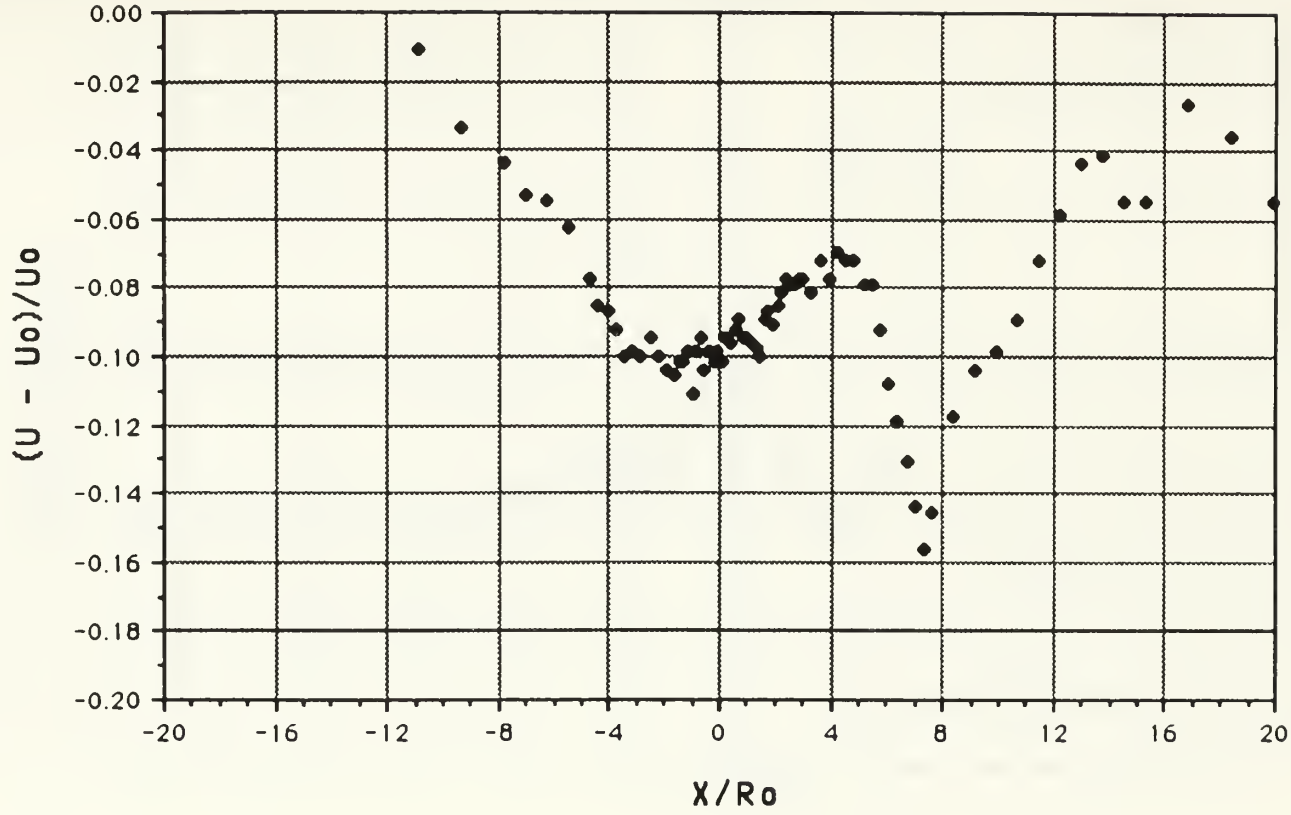

Figure 18. Axial Velocity Defect versus Radial Distance for $h_1/h_o = 1.6$ and $h_o/\sigma_o = 3.85$

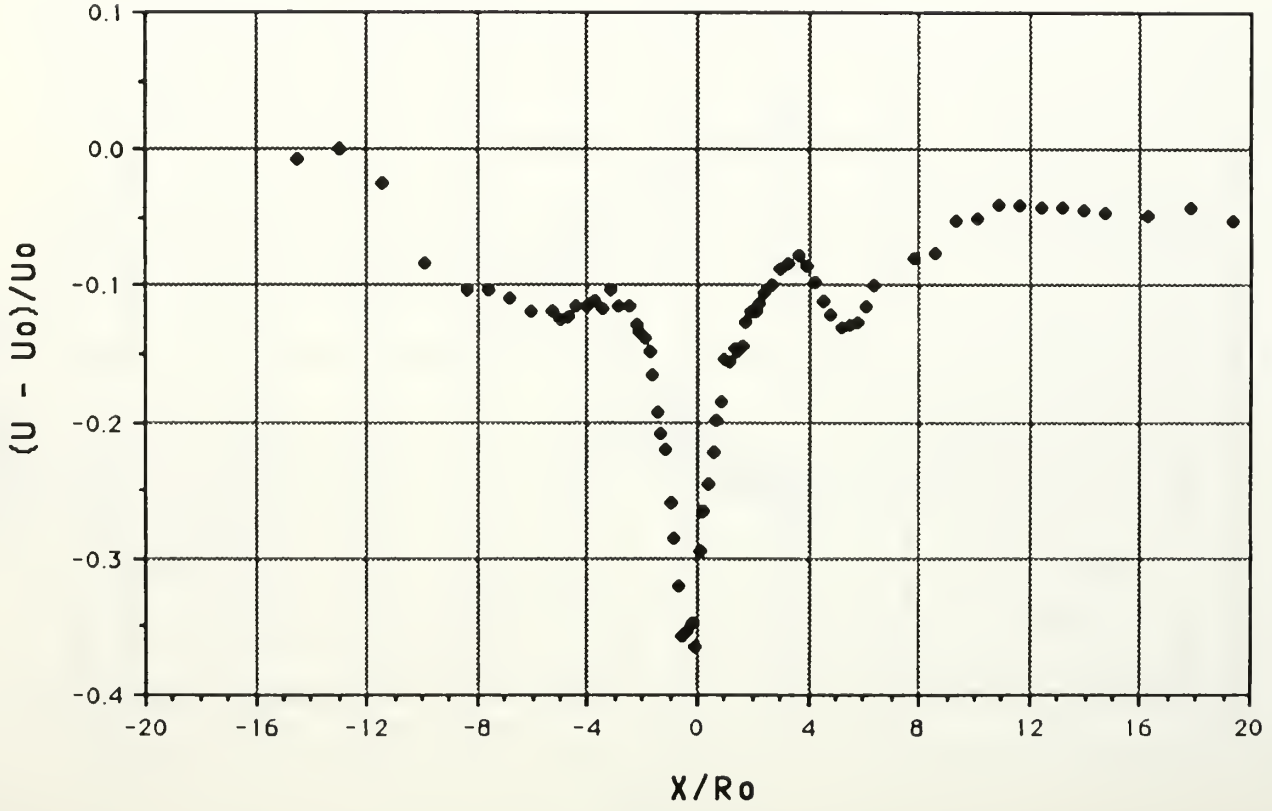

Figure 19. Axial Velocity Defect versus Radial Distance for $h_1/h_o = 1.0$ and $h_o/\sigma_o = 3.85$

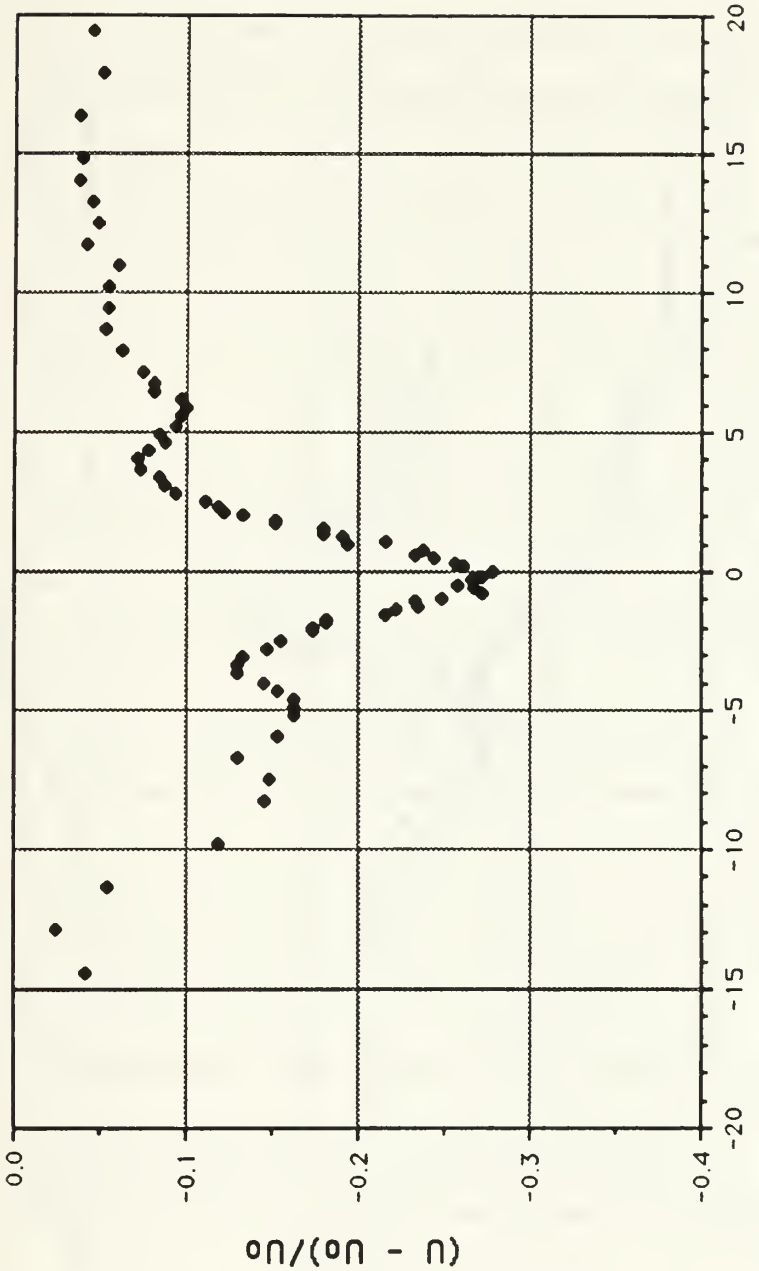

Figure 20. Axial Velocity Defect versus Radial Distance for $h_1/h_o = 0.8$ and $h_o/\sigma_o = 3.85$

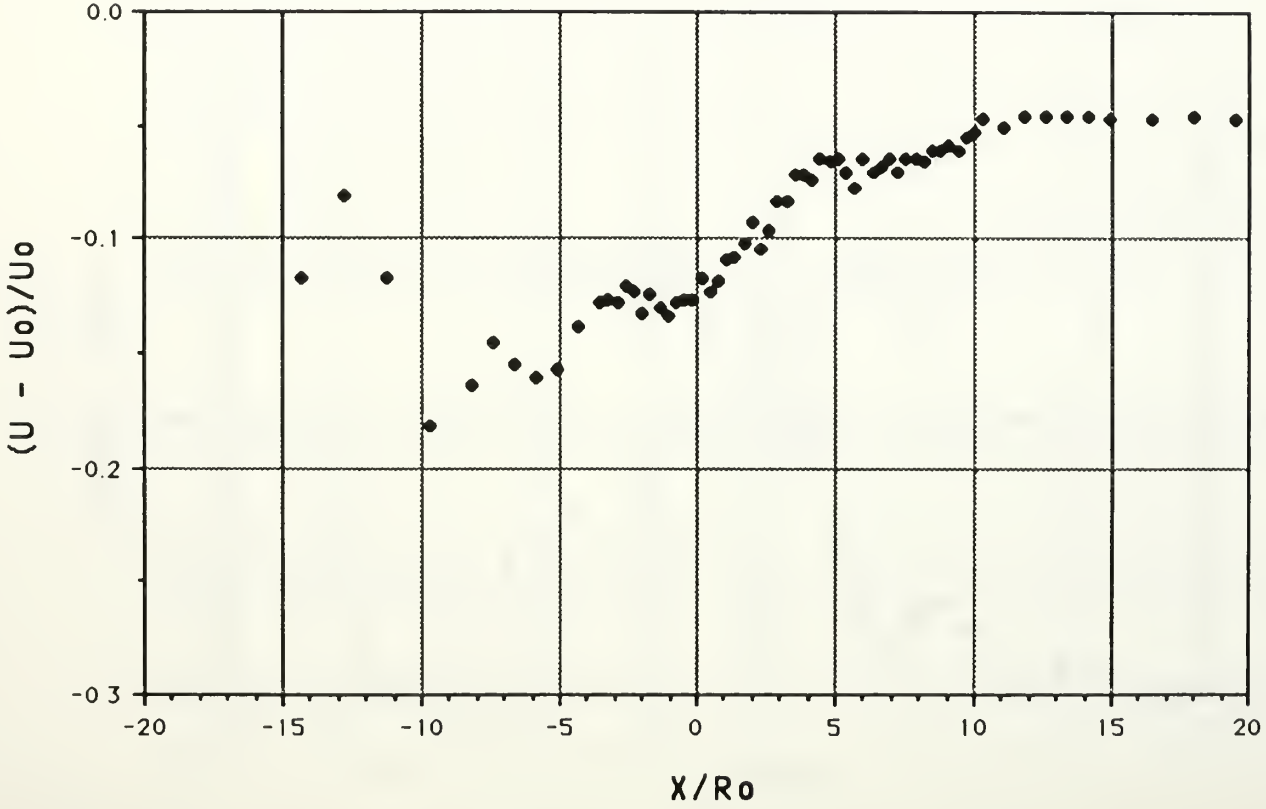

Figure 21. Axial Velocity Defect versus Radial Distance for $h_1/h_o = 0.4$ and $h_o/\sigma_o = 3.85$

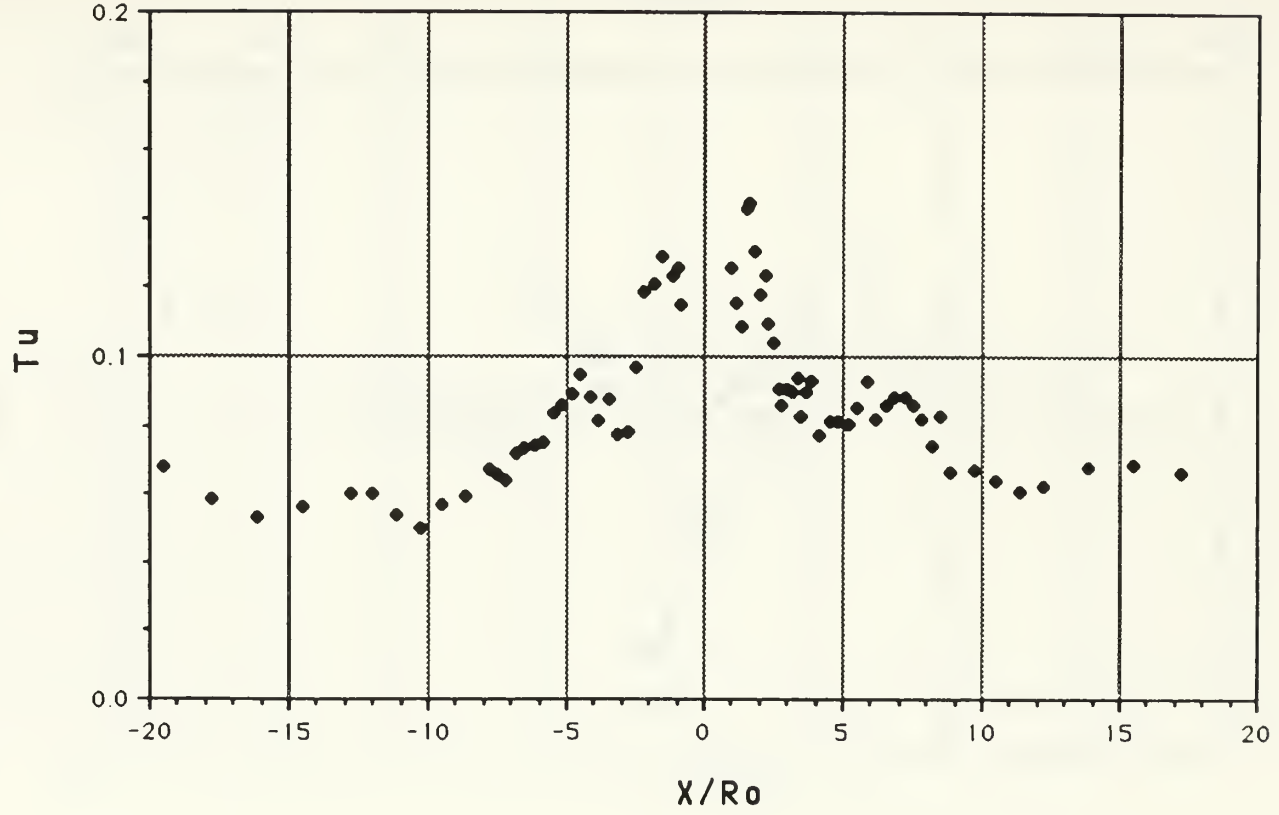

Figure 22. RMS Value of v' versus Radial Distance for $h_1/h_o = 1.0$ and $h_o/\sigma_o = 8.3$

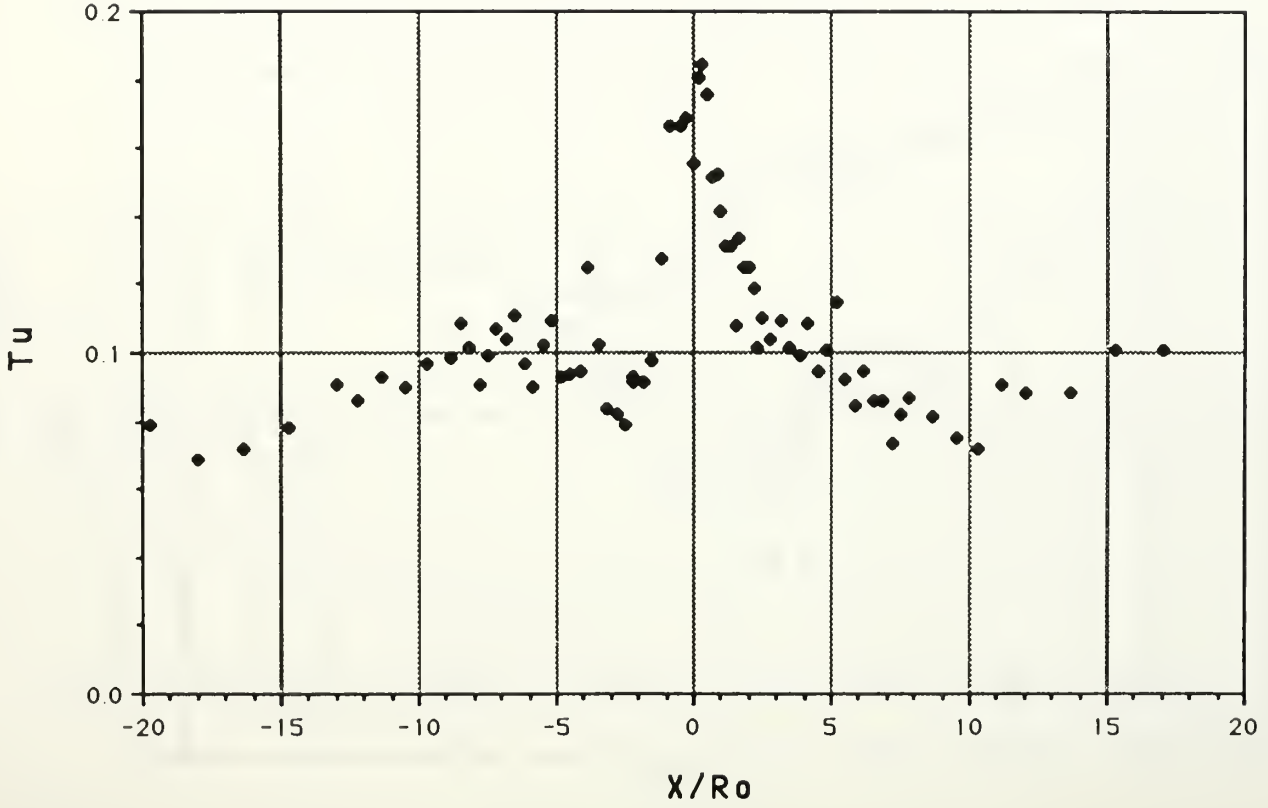

Figure 23. RMS Value of v' versus Radial Distance for $h_1/h_o = 0.8$ and $h_o/\sigma_o = 8.3$

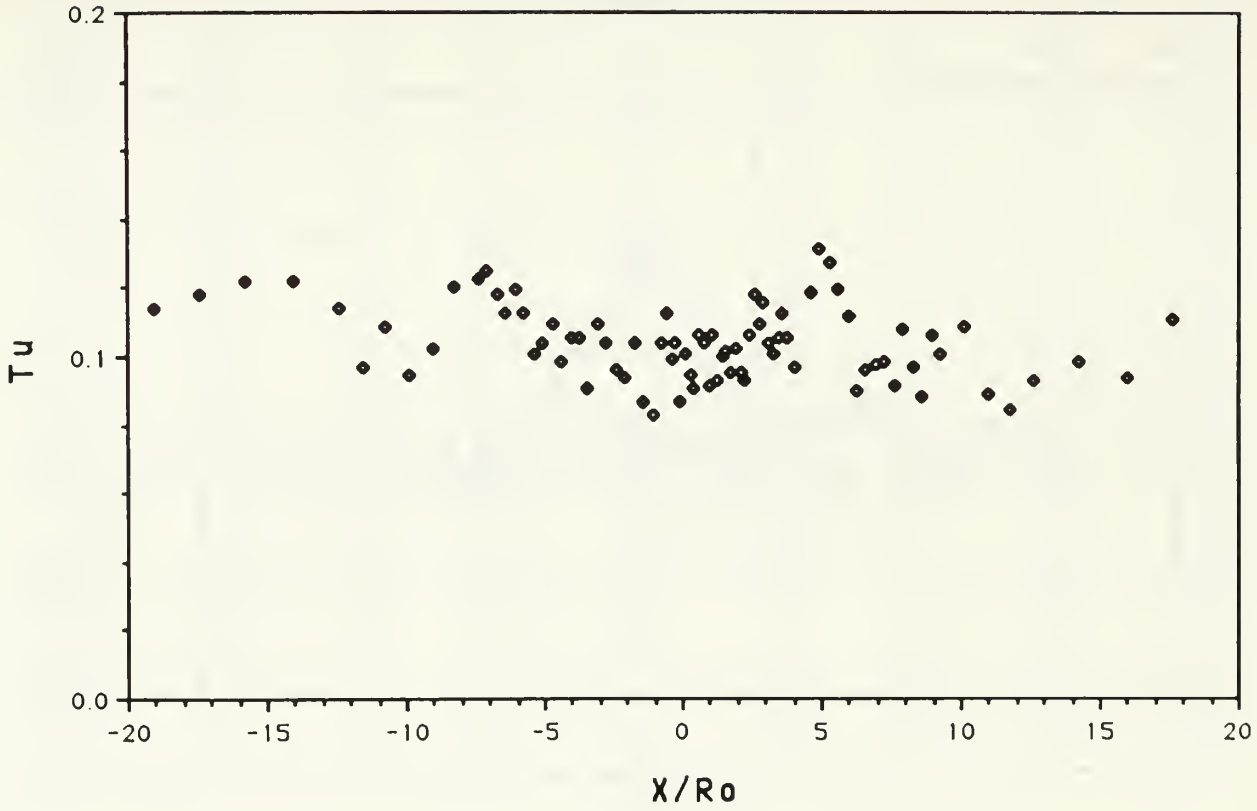

Figure 24. RMS Value of v' versus Radial Distance for $h_1/h_o = 0.4$ and $h_o/\sigma_o = 8.3$

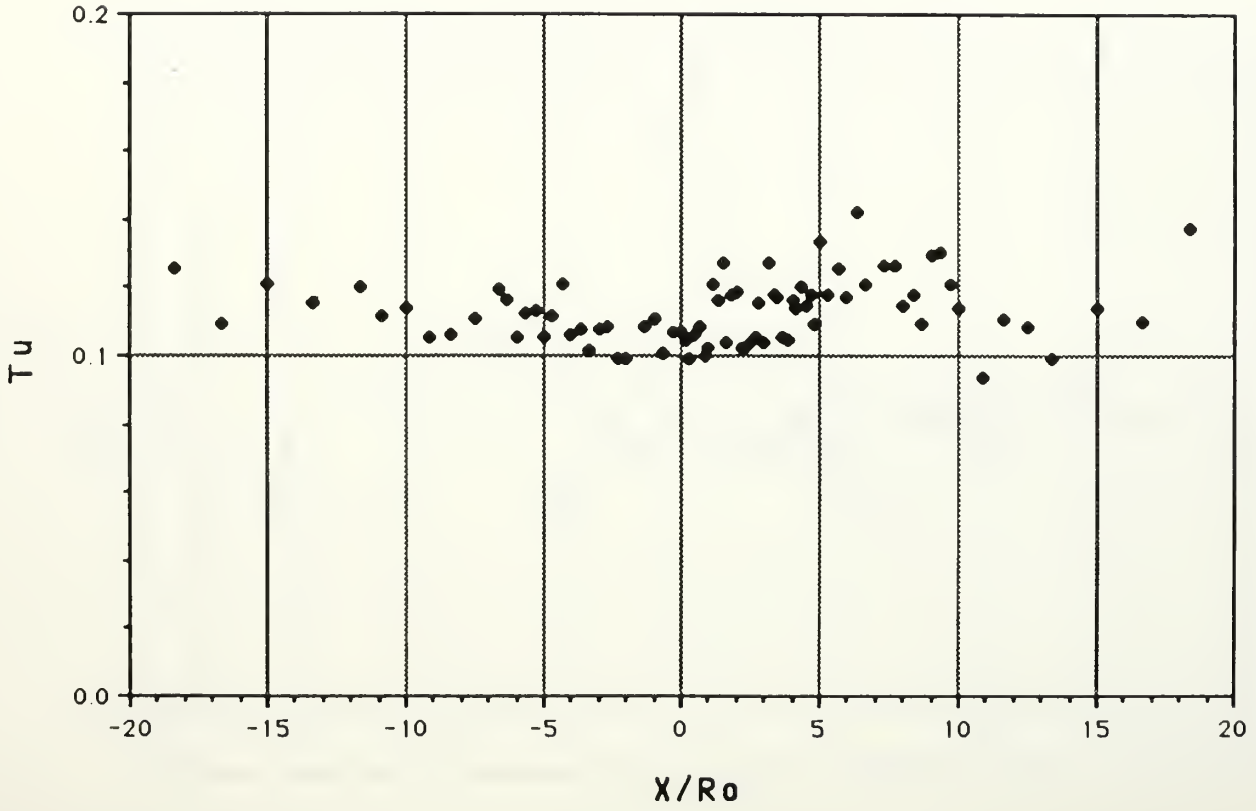

Figure 25. RMS Value of v' versus Radial Distance for $h_1/h_o = 0.2$ and $h_o/\sigma_o = 8.3$

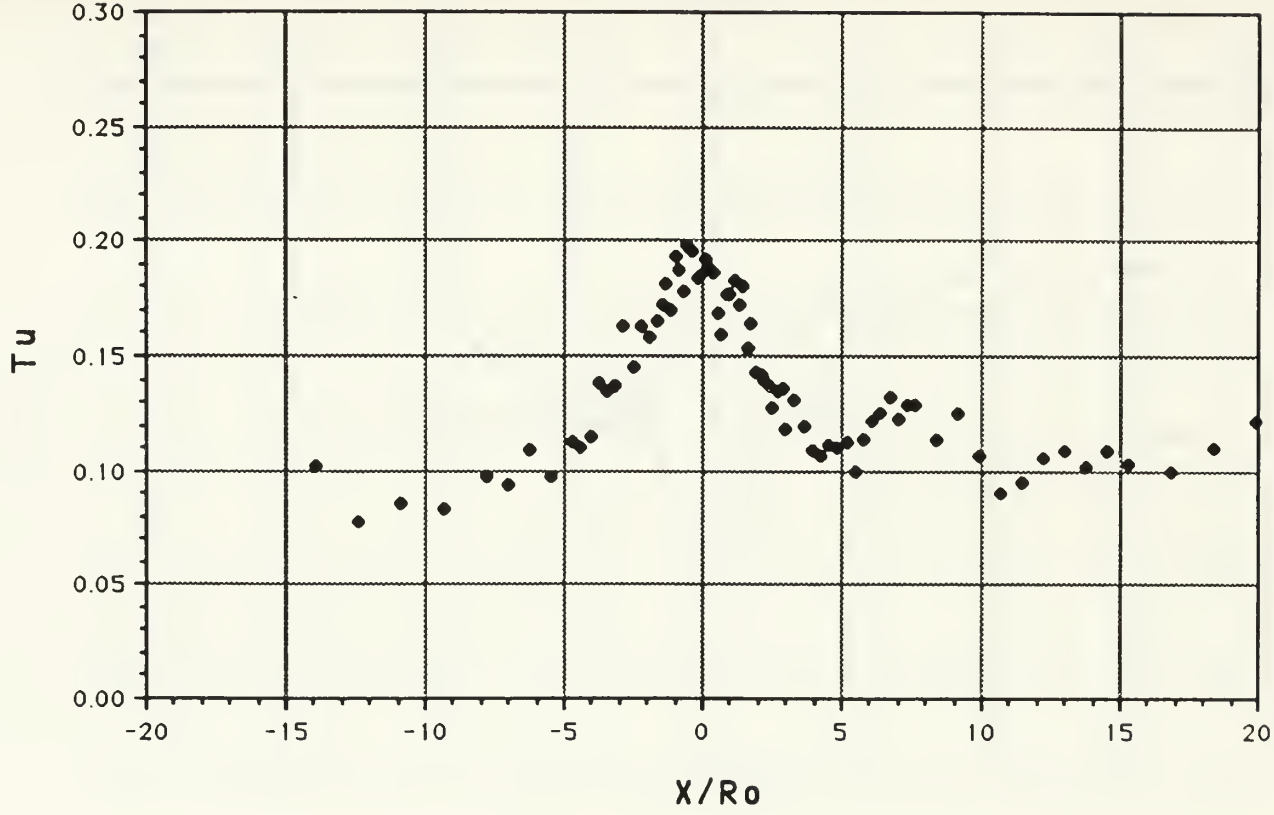

Figure 26. RMS Value of v' versus Radial Distance for h_1/h_o = 1.6 and h_o/σ_o = 3.85

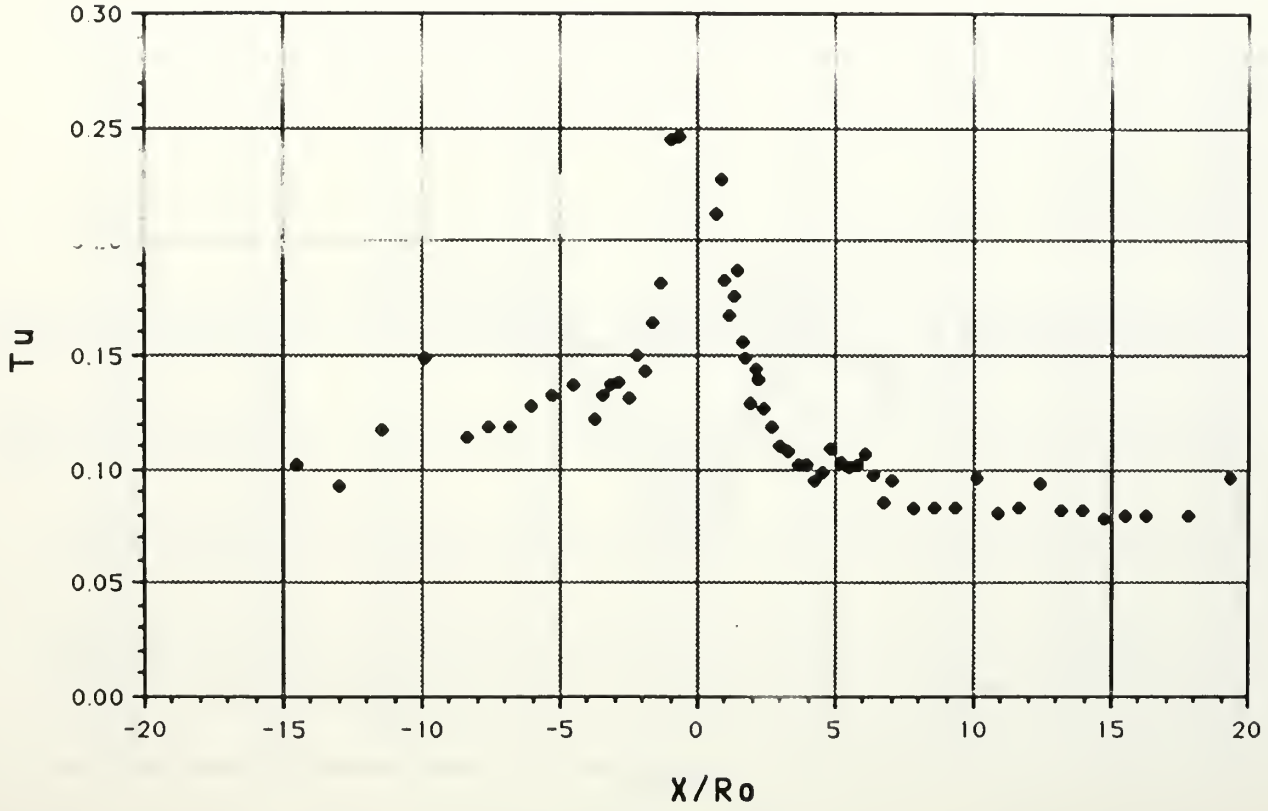

Figure 27. RMS Value of v' versus Radial Distance for $h_1/h_o = 1.0$ and $h_o/\sigma_o = 3.85$

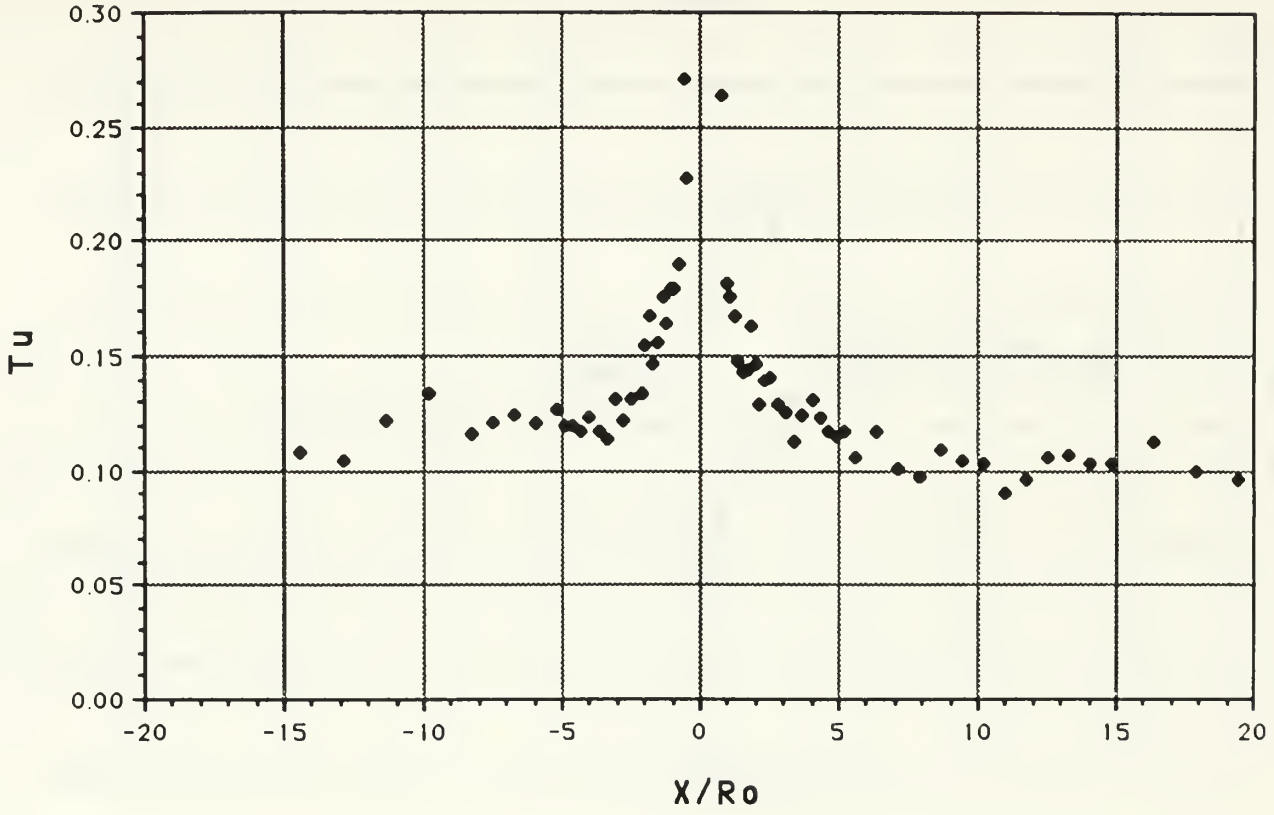

Figure 28. RMS Value of v' versus Radial Distance for $h_1/h_o = 0.8$ and $h_o/\sigma_o = 3.85$

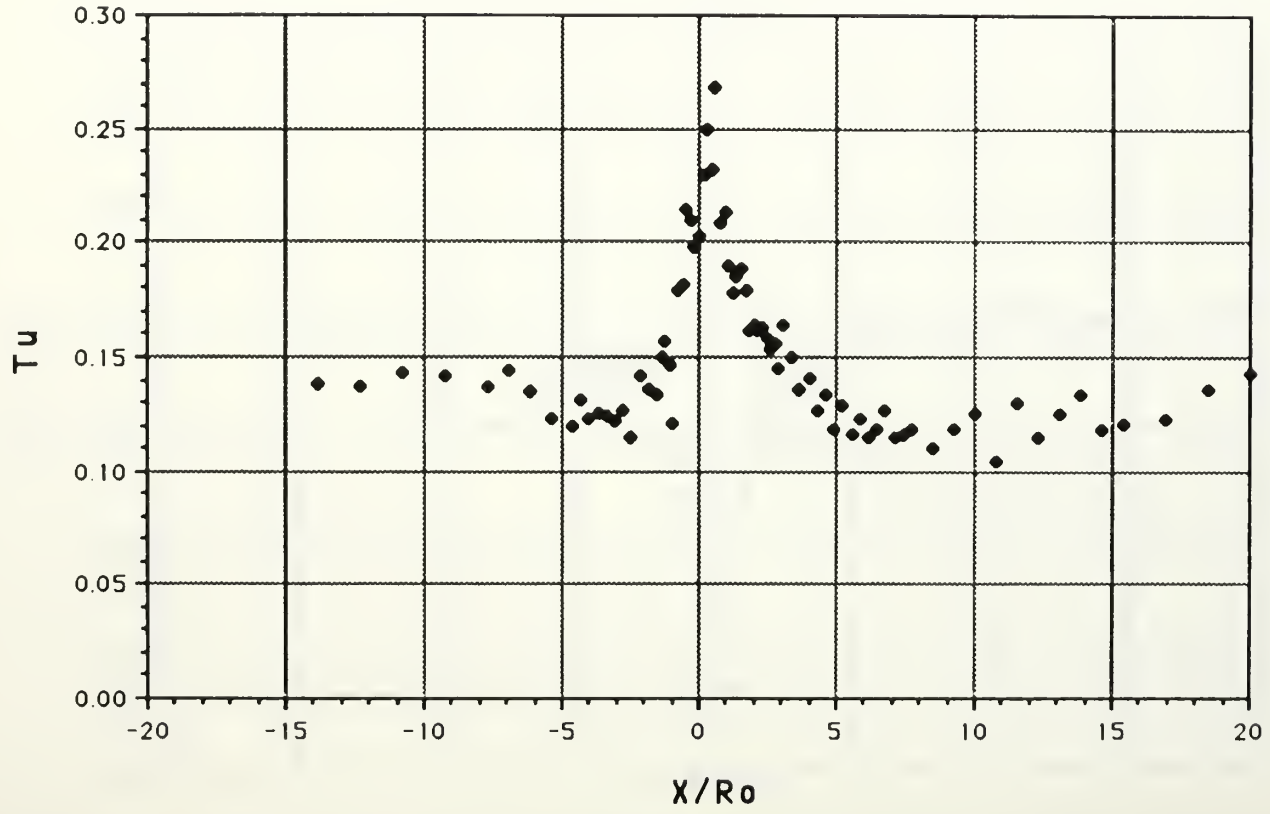

Figure 29. RMS Value of v' versus Radial Distance for h_1/h_o = 0.6 and h_o/σ_o = 3.85

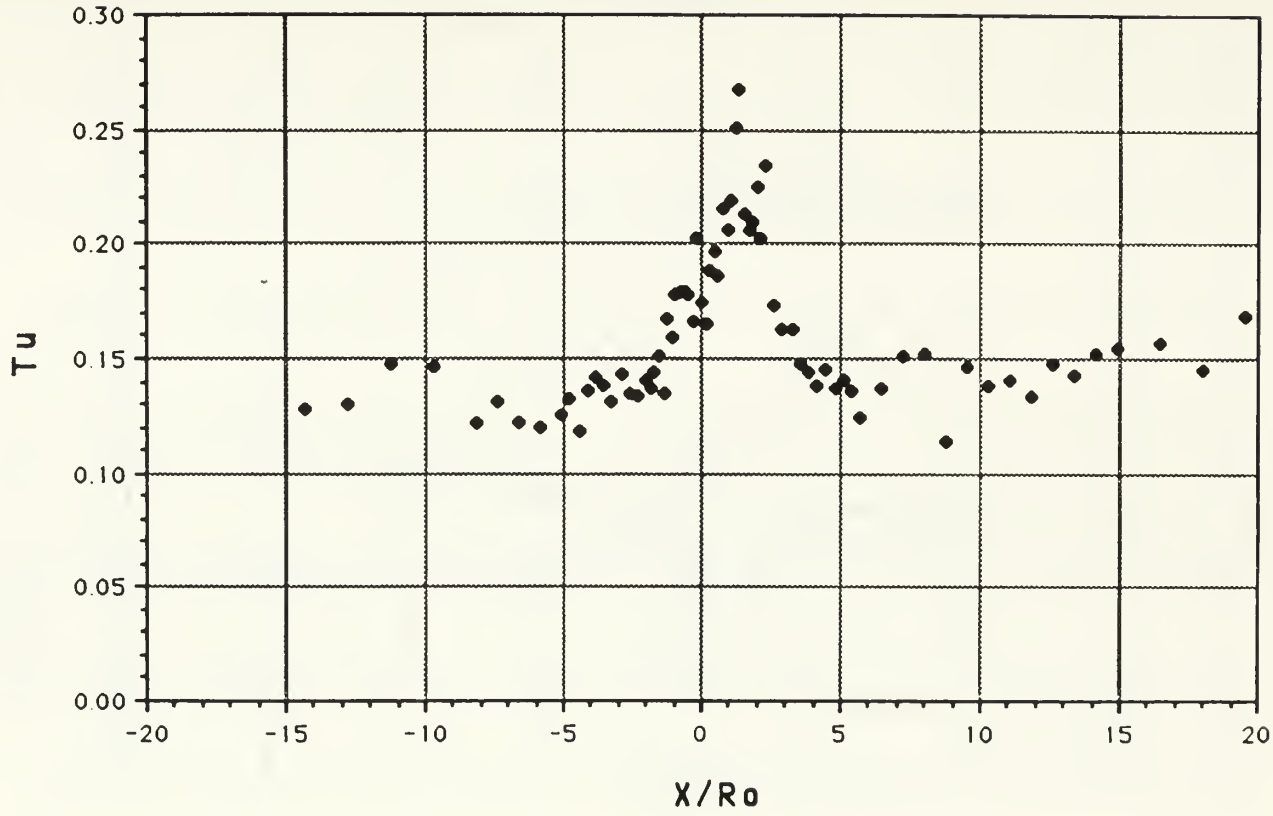

Figure 30. RMS Value of v' versus Radial Distance for $h_1/h_o = 0.4$ and $h_o/\sigma_o = 3.85$

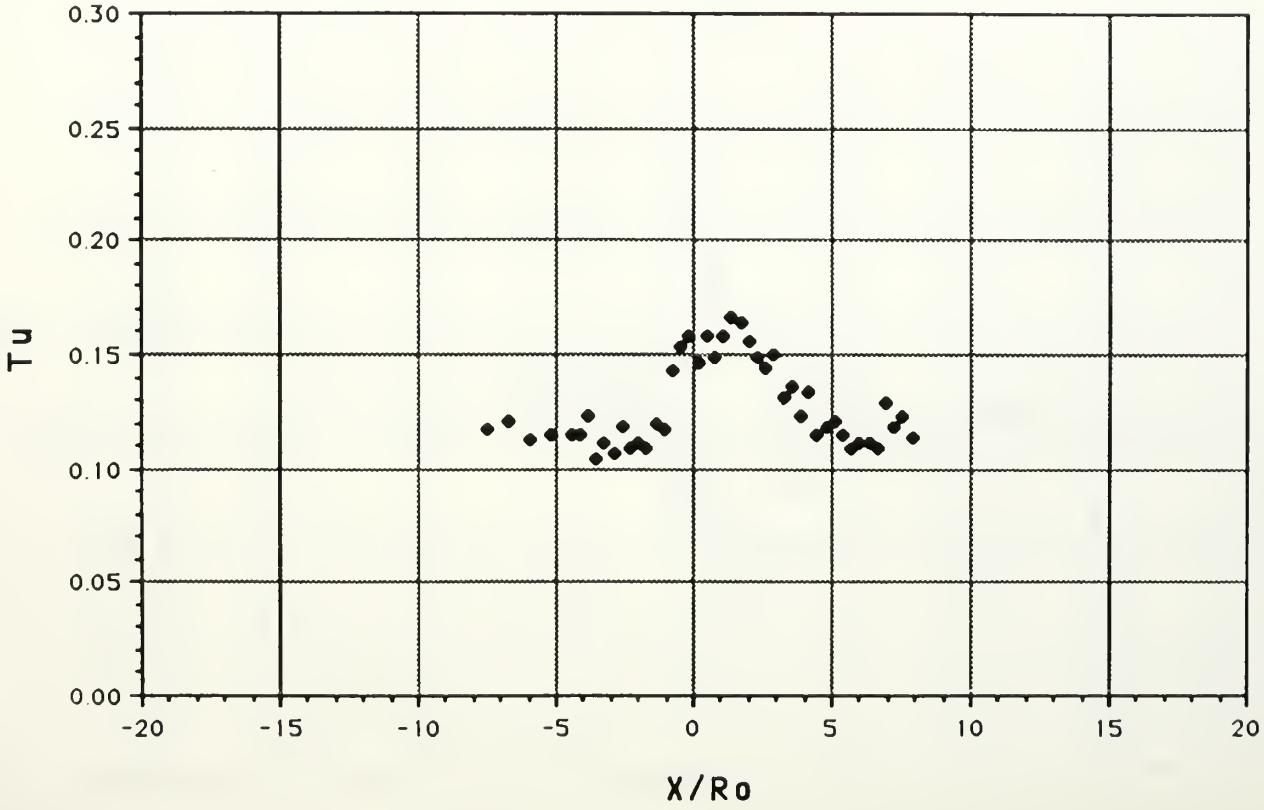

Figure 31. RMS Value of v' versus Radial Distance for h_1/h_o = 0.36 and h_o/σ_o = 3.85

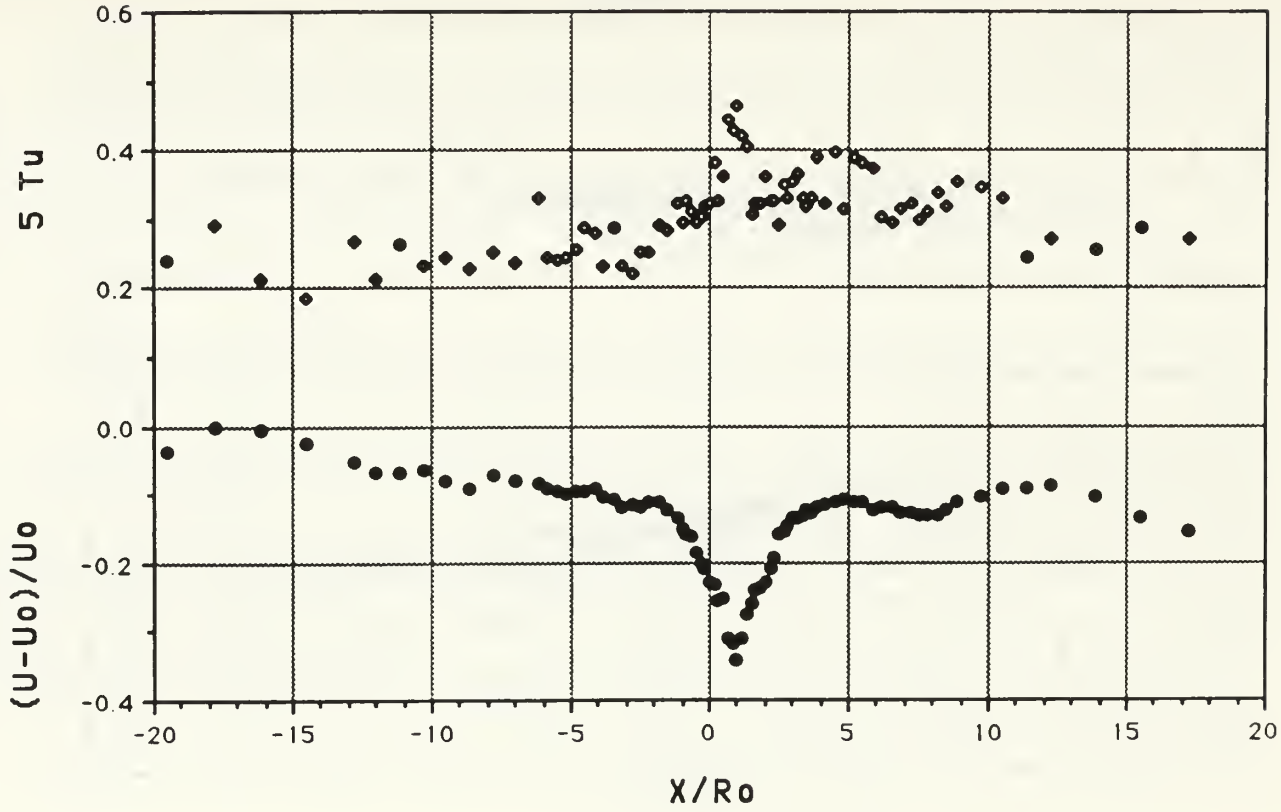

Figure 32. The RMS Value of u' and the Axial Velocity Defect for $h_1/h_o = 1.0$ and $h_o/\sigma_o = 8.3$

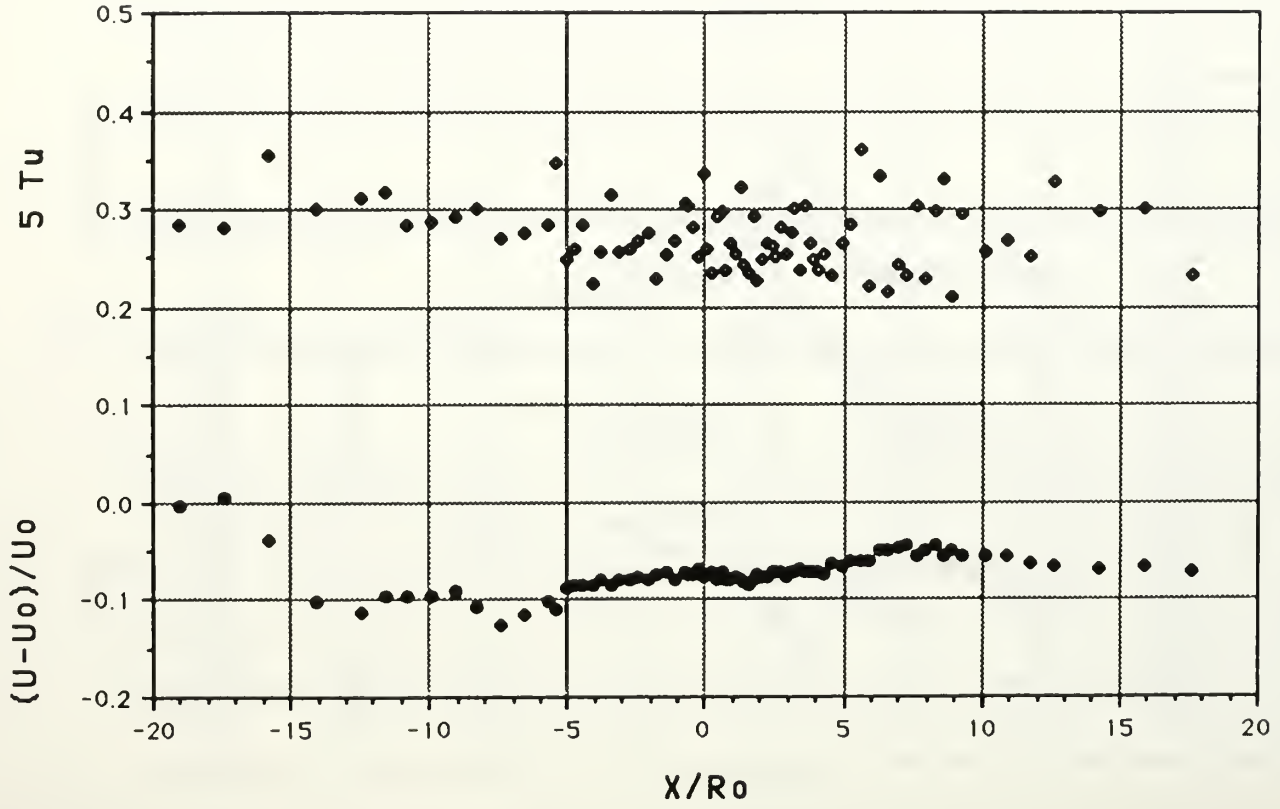

Figure 33. The RMS Value of u' and the Axial Velocity Defect for $h_1/h_o = 0.4$ and $h_1/\sigma_o = 8.3$

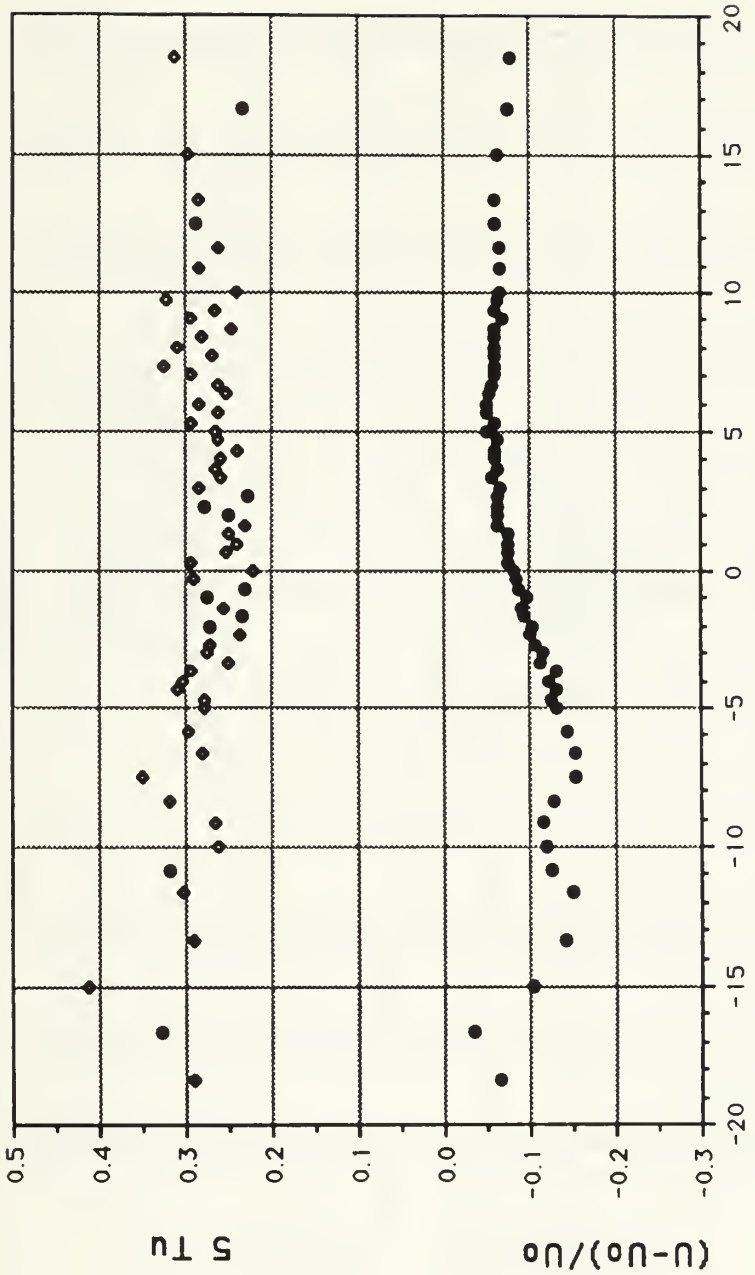

Figure 34. The RMS Value of u' and the Axial Velocity Defect for $h_1/h_o = 0.2$ and $h_o/\sigma_o = 8.3$

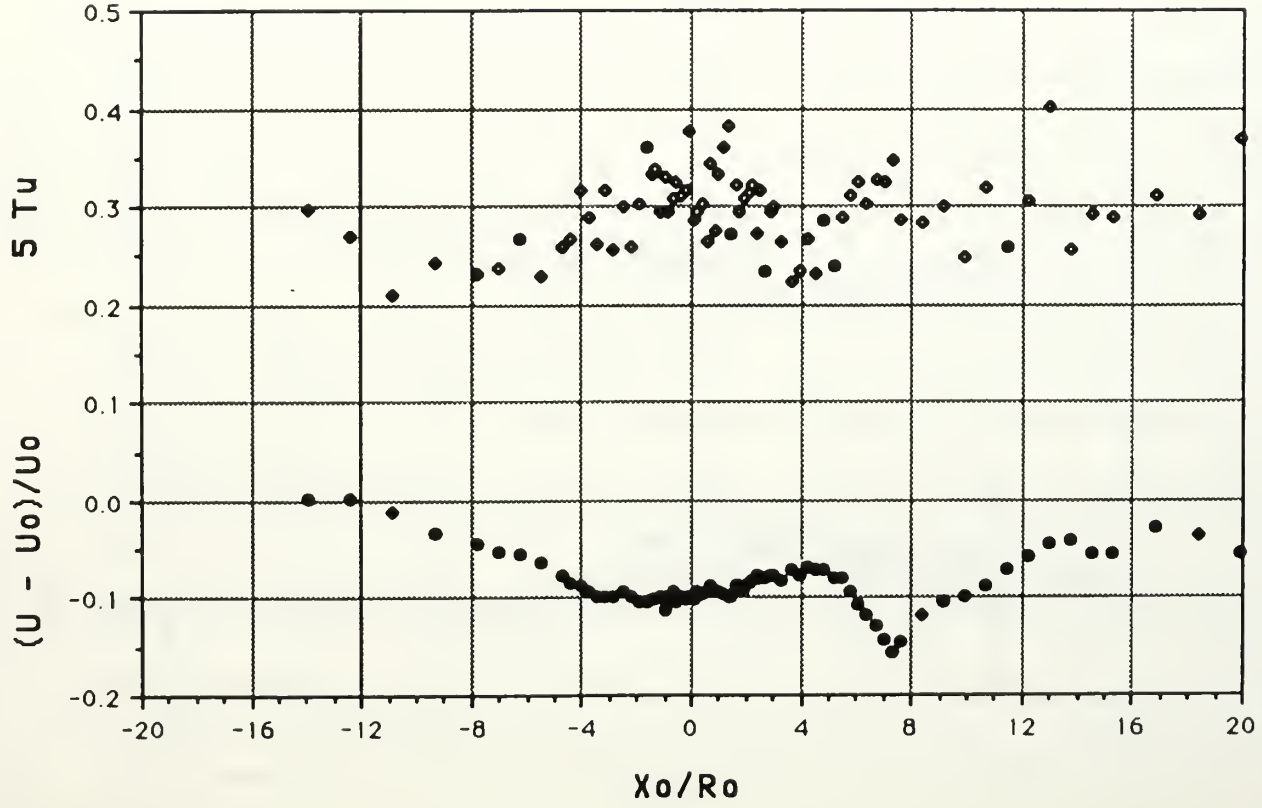

Figure 35. The RMS Value of u' and the Axial Velocity Defect for $h_1/h_o = 1.6$ and $h_o/\sigma_o = 3.85$

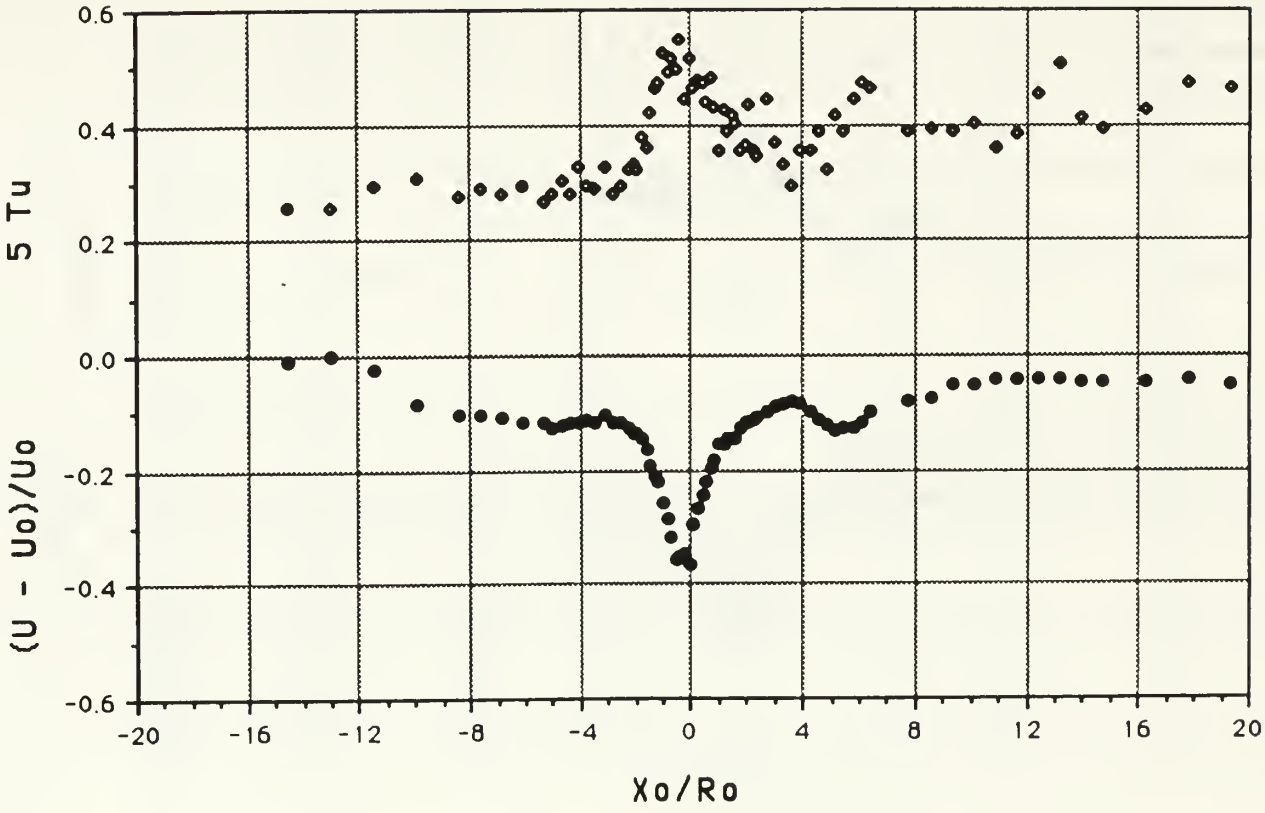

Figure 36. The RMS Value of u' and the Axial Velocity Defect for $h_1/h_o = 1.0$ and $h_o/\sigma_o = 3.85$

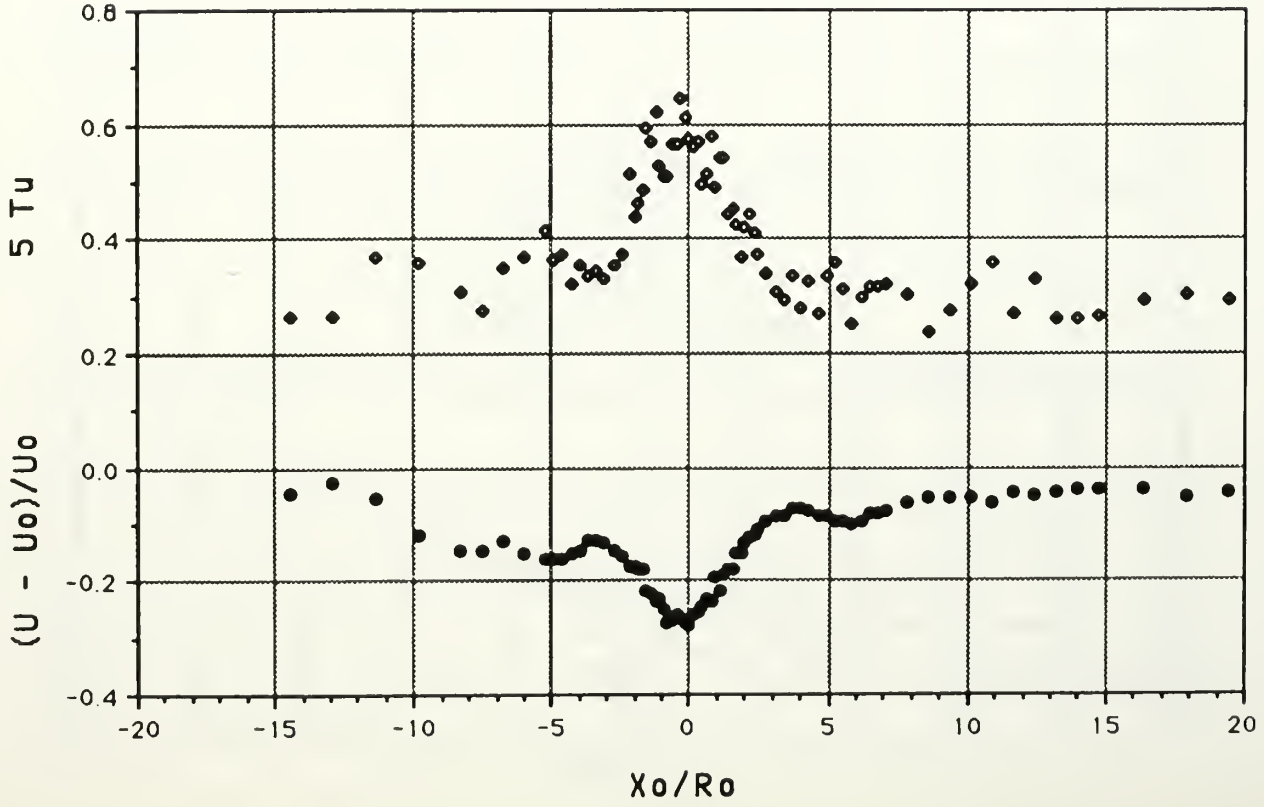

Figure 37. The RMS Value of u' and the Axial Velocity Defect for $h_1/h_o = 0.8$ and $h_o/\sigma_o = 3.85$

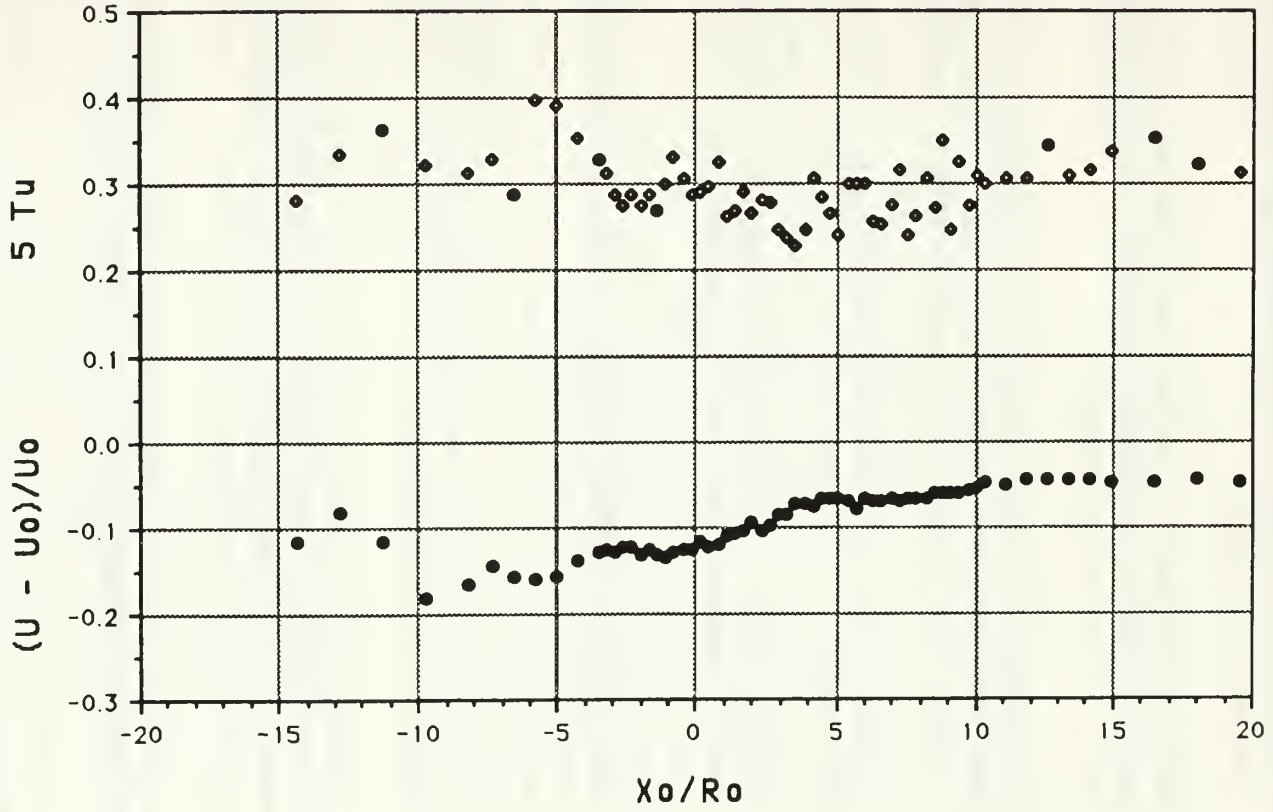

Figure 38. The RMS Value of u' and the Axial Velocity Defect for $h_1/h_o = 0.4$ and $h_o/\sigma_o = 3.85$

REFERENCES

1. Anthony, D. G., 1990, "The Influence of a Free Surface on the Development of Turbulence in a Submerged Jet," Technical Report No. 90-2, The University of Michigan.

2. Baker, G. R., Barker, S. J., Bofah, K. K., and Saffman, P. G., 1974, "Laser Anemometer Measurements of Trailing Vortices," *Journal of Fluid Mechanics*, Vol. 65, pp. 325-336.

3. Bandyopadhyay, P. R., Stead, D. J., and Ash, R. L., 1990, "The Organized Nature of a Turbulent Trailing Vortex," AIAA 90-1625, 21st *Fluid Dynamics, Plasma Dynamics and Lasers Conference, Seattle, WA.*

4. Batchelor, G. K., 1964, "Axial Flow in Trailing Line Vortices," *Journal of Fluid Mechanics*, Vol. 20, pp. 645-658.

5. Corsiglia, V. R., Schwind, R. G., and Chigier, N. A., 1973, "Rapid Scanning, Three-Dimensional Hot-Wire Anemometer Surveys of Wing-Tip Vortices," *Journal of Aircraft*, Vol. 10, pp. 752-757.

6. Crow, S. C., 1970, "Stability Theory for a Pair of Trailing Vortices," *AIAA Journal*, Vol. 8, No. 12, pp. 2172–2179.

7. Dommermuth, D. G., 1992, "The Formation of U-Shaped Vortices on Vortex Tubes Impinging on a Wall with Applications to Free Surfaces," (to appear in *Physics of Fluids* A).

8. Dommermuth, D. G. and Yue, D. K., 1991, "A Numerical Study of Three-Dimensional Viscous Interaction of Vortices with a Free Surface," *Proceedings of the 18th Symposium on Naval Hydrodynamics*, National Academy Press, Washington, D.C., pp. 727-788.

9. Evans, J. T., 1955, "Pneumatic and Similar Breakwaters," *Proceedings of the Royal Society of London* , Vol. A-231, pp. 457-466.

10. Durand, W. F. (ed.), 1963, *Aerodynamic Theory*, Vol. III, pp. 280-306. Dover.

11. Elnitsky II, J., 1987, *Interaction of a Vortex Pair With a Free Surface*, M.S. and Engineer Degree Thesis, Naval Postgraduate School, Monterey, California.

12. Green, S. I. and Acosta, A. J., 1991, "Unsteady Flow in Trailing Vortices," *Journal of Fluid Mechanics*, Vol. 227, pp. 107-134.

13. Harvey, J. K. and Perry, F. J., 1971, "Flow Field Produced by Trailing Vortices in the Vicinity of the Ground," *AIAA Journal*, Vol. 9, pp. 1659-1660.

14. Higuchi, H., Quadrelli, J. C., and Farrell, C., 1987, "Vortex Roll-Up from an Elliptical Wing at Moderately Low Reynolds Numbers," *AIAA J.*, Vol. 25, pp. 1537-1542.

15. Hirsa, A., Tryggvason, G., Abdollahi-Alibeik, J., Willmarth, W. W., 1991, "Measurement and Computations of Vortex Pair Interaction with a Clean or Contaminated Free Surface," *Proceedings of the 18th Symposium on Naval Hydrodynamics*, National Academy Press, Washington, D.C., pp. 521-531.

16. Komori, S., Ueda, H., Ogino, F., and Mizushima, T., 1982, "Turbulence Structure and Transport Mechanism at the Free Surface in an Open Channel Flow," *International Journal of Heat and Mass Transfer*, Vol. 25(4), pp. 513-521.

17. Kwon, J. T., 1989, "Experimental Study of Vortex Ring Interaction with a Free Surface," Ph. D. Thesis, 1989, The University of Michigan.

18. Lamb, H. (Sir), 1945, *Hydrodynamics*, 6th ed., Dover Publications, NY, pp. 221–224.

19. Langmuir, I., 1938, "Surface Motion of Water Induced by Wind," *Science*, Vol. 87, pp. 119–123.

20. Madnia, K. and Bernal, L. P., 1989, "Interaction of a Turbulent Round Jet with the Free Surface," Technical Report No. 89-05, The University of Michigan.

21. Marcus, D. L., and Berger, S. A., 1989, "The Interaction Between a Counter-Rotating Vortex Pair in Vertical Ascent and a Free Surface," *Physics of Fluids*, A-1, Vol. 12, pp. 1988–2000.

22. Moore, D. W. and Saffman, P. G., 1973, "Axial Flow in Laminar Trailing Vortices," *Proceedings of the Royal Society of London*, Vol. A 333, pp. 491-508.

23. Ohring, S., and Lugt, H. J., 1991, "Interaction of a Viscous Vortex Pair with a Free Surface," *Journal of Fluid Mechanics*, Vol. 227, pp. 47-70.

24. Peace, A. J. and Riley, N., 1983, "A Viscous Vortex Pair in Ground Effect," *Journal of Fluid Mechanics*, Vol. 129, pp. 409-426.

25. Ramberg, S. E., Swean, T. F., and Plesnia, M. W., 1989, "Turbulence Near a Free Surface in a Plane Jet," Naval Research Laboratory Memorandum Report 6367.

26. Sarpkaya, T., 1983, "Trailing Vortices in Homogeneous and Density Stratified Media," *Journal of Fluid Mechanics*, Vol. 136, pp. 85–109.

27. Sarpkaya, T., 1985, "Surface Signatures of Trailing Vortices and Large Scale Instabilities," *Proceedings of the Colloquium on Vortex Breakdown*, (ed. R. W. Staufenbiel), pp. 145-187, Aachen, Germany.

28. Sarpkaya, T., 1986, "Trailing-Vortex Wakes on the Free Surface," *Proceedings of the 16th Symposium on Naval Hydrodynamics*, National Academy Press, Washington, D. C., pp. 38–50.

29. Sarpkaya, T., 1992, "Interaction of a Turbulent Vortex with a Free Surface," Proceedings of the Nineteenth Symposium on Naval Hydrodynamics, Vol. 1, pp. 163-174.

30. Sarpkaya, T., Elnitsky, J., and Leeker, R. E., 1988, "Wake of a Vortex Pair on the Free Surface," *Proceedings of the 17th Symposium on Naval Hydrodynamics*, National Academy Press, Washington, D. C., pp. 47–54.

31. Sarpkaya, T., and Henderson, D. O., Jr., 1984, *Surface Disturbances Due to Trailing Vortices*, Technical Report No. NPS-69-84-004, Naval Postgraduate School, Monterey, California.

32. Sarpkaya, T., and Henderson, D. O., Jr., 1985, "Free Surface Scars and Striations Due to Trailing Vortices Generated by a Submerged Lifting Surface," AIAA 85-0445, presented at the 23rd Aerospace Sciences Meeting, Reno, Nevada, 14–17 January 1985.

33. Sarpkaya, T., and Suthon, P. B. R., 1991a, "Interaction of a vortex couple with a free surface," *Experiments in Fluids*, Vol. 11, pp. 205-217.

34. Sarpkaya, T., and Suthon, P. B. R., 1991b, "Scarred and Striated Signature of a Vortex Pair on the Free Surface," *Proceedings of the l8th Symposium on Naval Hydrodynamics*, National Academy Press, Washington, D. C., pp. 503-519.

35. Scott, J. C., 1982, "Flow Beneath a Stagnant Film on Water, The Reynolds Ridge," *Journal of Fluid Mechanics*, Vol. 116, pp. 283–296.

36. Singh, P. I. and Uberoi, M. S., 1976, "Experiments on Vortex Stability," *Physics of Fluids*,, Vol. 19, pp. 1181-1188.

37. Smith, C. R., Walker, J. D. A., Haidari, A. H., and Sobrun, U., 1991, "On the Dynamics of Near-Wall Turbulence," *Phil. Trans. Royal Soc. London* A, Vol. 336, pp. 131-175.

38. Stinebring, D. R., Farrell, K. J., and Billet, M. L., 1989, "Structure of a Tip Vortex Trailing from a Three-Dimensional Hydrofoil," *Proceedings of the 22nd American Towing Tank Conf.*, St. John's, Canada.

39. Telste, J. G., 1989, "Potential Flow about Two Counter-Rotating Vortices Approaching a Free Surface," *Journal of Fluids Mechanics*, Vol. 201, pp. 259–278.

INITIAL DISTRIBUTION LIST

		No. Copies
1.	Defense Technical Information Center Cameron Station Alexandria, VA 22304–6145	2
2.	Library, Code 52 Naval Postgraduate School Monterey, CA 93943-5002	2
3.	Department Chairman, Code ME Department of Mechanical Engineering Naval Postgraduate School Monterey, CA 93943-5000	1
4.	Professor T. Sarpkaya, Code ME-SL Department of Mechanical Engineering Naval Postgraduate School Monterey, CA 93943-5000	5
5.	LT Donald E. Neubert, Jr. 910 Marion Place Ridgefield, NJ 07657	2
6.	Curricular Officer, Code 34 Department of Naval Engineering Naval Postgraduate School Monterey, CA 93942-5000	1